Supplementary Information (SI) for Chemical Communications.

This journal is © The Royal Society of Chemistry 2026

Electronic Supplementary Information (ESI)

Synthesis and Characterizations of A π-Extended Nonbenzenoid Perylene

Laiyun Zhou, [†a] Yanru Bai, [†a, b] Yangyang Zhao, [b] Guanghua Liu, [c] Bin Rao, [b] Zhicheng Zhang *[b] and Qing Wang *[b]

[a] School of Chemistry and Chemical Engineering, Inner Mongolia University, Hohhot 010021, P. R. China

[b] School of Chemistry, Xi' an Jiaotong University, Engineering Research Center of Energy Storage Materials and Devices, Ministry of Education, Xi' an, Shaanxi, 710049, P. R. China

[c] Institute of Agricultural and Livestock Product Quality, Inner Mongolia Academy of Agricultural and Animal Husbandry Sciences, Hohhot 010030, P. R. China

*Corresponding author. E-mail:wangqing0114@xjtu.edu.cn; zhichengzhang@mail.xjtu.edu.cn

Table of contents

1. Experimental Section

1.1 General

All reagents and starting materials were obtained from commercial suppliers and used without further purification unless otherwise noted. Anhydrous toluene and THF were distilled from sodium-benzophenone immediately prior to use. Anhydrous dichloromethane (DCM) and acetonitrile (MeCN) were distilled from CaH_2. All reaction conditions dealing with air and moisture sensitive compounds were carried out in a dry reaction vessel under nitrogen atmosphere. All reaction conditions dealing with air and moisture-sensitive compounds, including the generation of radical cations and anions during chemical titrations, were carried out in a dry reaction vessel under a nitrogen atmosphere using anhydrous solvents. Cyclic voltammetry measurements were performed in dry dichloromethane (DCM) The solution was deaerated with bubbling nitrogen prior to measurement. ^{1}H and ^{13}C NMR spectra were recorded using Bruker Advance II 600MHz spectrometer in $CDCl_3$, using tetramethylsilane (TMS) as the internal standard. The chemical shift was recorded in ppm and the following abbreviations were used to explain the multiplicities: s = singlet, d = doublet, t = triplet, m = multiplet. APCI mass spectra were recorded on a SHIMADZU/LCMS-IT-TOF instrument. UV/Vis absorption was recorded on a SHIMADZU UV-3600i spectrophotometer. Steady-state photoluminescence (PL) spectra were recorded on a HITACHI F-4700 spectrophotometer. Cyclic voltammetry measurements were performed in dry dichloromethane (DCM) on a CHI 620C electrochemical analyzer with a three-electrode cell, using 0.1 M Bu_4NPF_6 as supporting electrolyte, AgCl/Ag as reference electrode, gold disk as working electrode (2 mm diameter, polished with a polishing cloth containing Al_2O_3 powder (particle size 0.05 μm), Pt as counter electrode. The solution was deaerated with bubbling nitrogen prior to measurement. Single crystals were measured at low temperature on a Bruker D8 VENTURE Metaljet PHOTON II diffractometer. Continuous wave X-band EPR spectra were obtained with a Bruker (EMX Plus) spectrometer.

1.2. Synthetic procedures and characterization data

Scheme S1. Synthetic route to **Pery-56**.

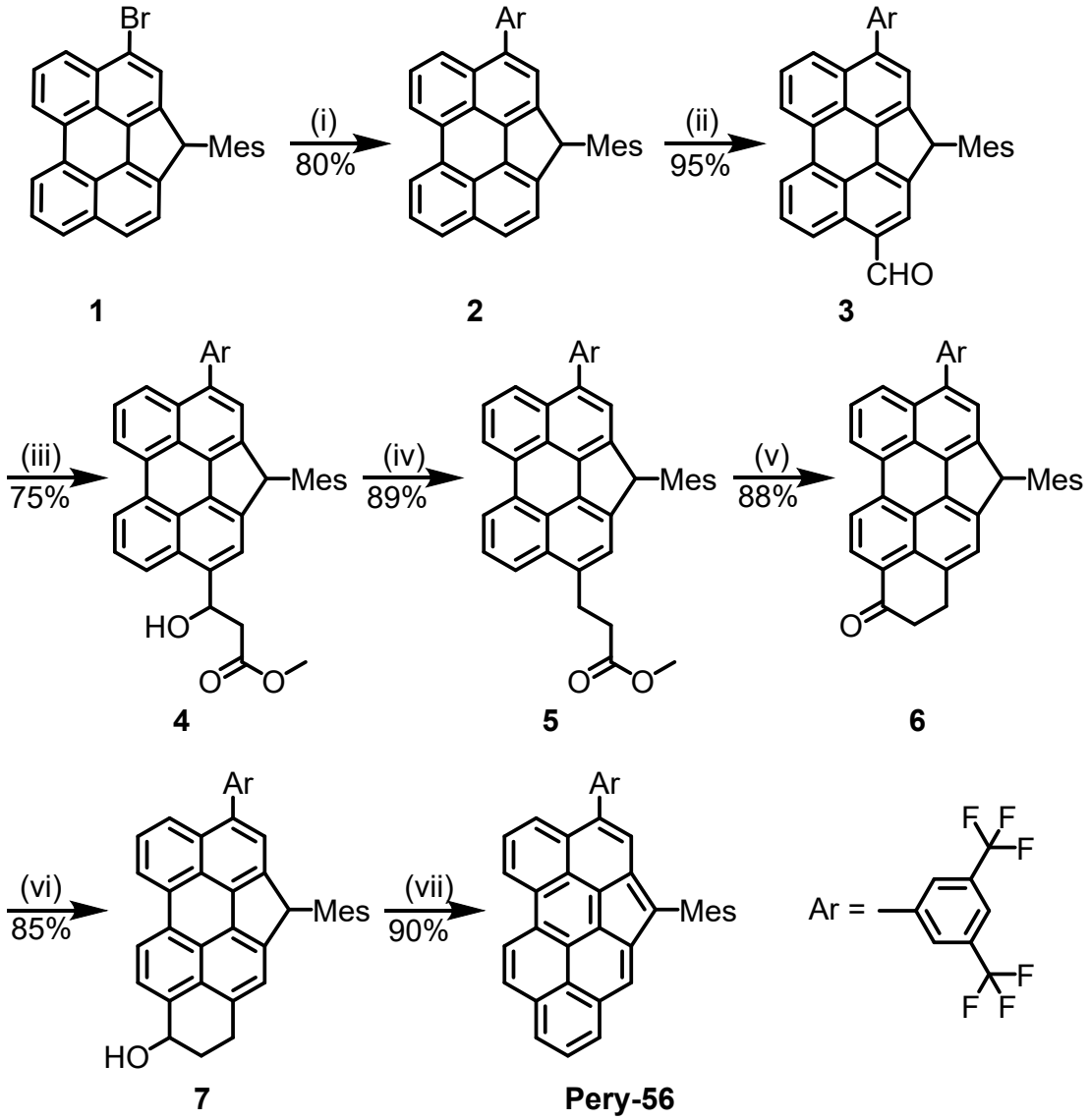

Reagents and conditions: (i) 2-(3,5-Bis(trifluoromethyl)phenyl)-4,4,5,5-tetramethyl-1,3,2-dioxaborolane, $Pd(PPh_3)_4$, Na_2CO_3, Ethanol (EtOH), Toluene (Tol); (ii) CH_3OCHCl_2, $SnCl_4$, Dichloromethane (DCM); (iii) Methyl bromoacetate, Zn, Chlorotrimethylsilane (TMSCl), Tetrahydrofuran (THF); (iv) Triethylsilane (Et_3SiH), Trifluoromethanesulfonic acid (TfOH), Dichloromethane (DCM); (v) Trifluoromethanesulfonic acid (TfOH), Toluene (Tol); (vi) Lithium aluminum hydride ($LiAlH_4$), Tetrahydrofuran (THF); (vii) *p*-Toluenesulfonic acid monohydrate (*p*-$TsOH \cdot H_2O$), Toluene (Tol).

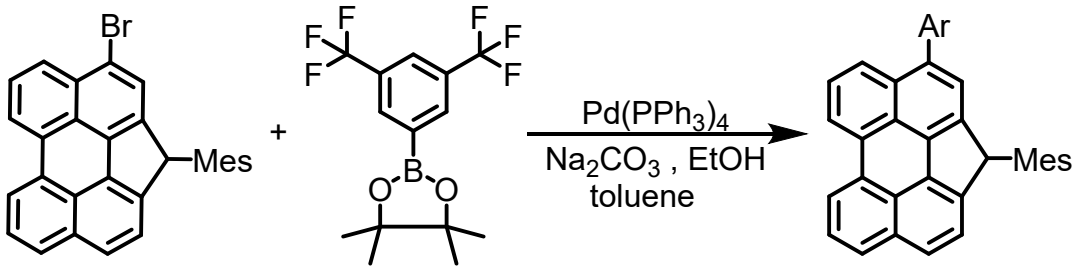

1 **2**

Synthesis of compound **2**: A double-necked round-bottom flask equipped with a magnetic stir bar was charged with **1** (2.16 g, 4.0 mmol), 2-(3,5-bis(trifluoromethyl)phenyl)-4,4,5,5-tetramethyl-1,3,2-dioxaborolane (3.40 g, 10.0 mmol), 2.0 M aqueous Na_2CO_3 (9.0 mL), ethanol (10.0 mL), and toluene (100 mL). $Pd(PPh_3)_4$ (580 mg, 25 mol%) was then added under a nitrogen atmosphere. The mixture was heated at 90 °C for 12 h. After cooling to room temperature, the reaction was quenched with water and extracted with organic solvent. The combined organic layers were concentrated under reduced pressure, and the residue was purified by column chromatography on silica gel using petroleum ether/DCM (20:1, v/v) as the eluent to afford compound **2** as yellow solid (2.58 g, 80%). ^{1}H NMR (400 MHz, $CDCl_3$) δ (ppm) =8.28 (t, *J* = 7.6 Hz, 2H), 8.00 (s, 2H), 7.91 (s, 1H), 7.86 (d, *J* = 8.2 Hz, 1H), 7.72 – 7.62 (m, 4H), 7.48 (d, *J* = 8.2 Hz, 1H), 7.41 (s, 1H), 7.08 (s, 1H), 6.68 (s, 1H), 5.53 (s, 1H), 2.80 (s, 3H), 2.30 (s, 3H), 1.15 (s, 3H).^{13}C NMR (101 MHz, $CDCl_3$) δ (ppm) = 143.53, 141.69, 140.78, 138.35, 138.00, 137.02, 136.89, 135.81, 134.98, 133.07, 132.88, 132.05, 132.03, 131.73, 131.27, 130.66, 130.38, 129.40, 128.28, 127.54, 126.92, 126.04, 125.97, 125.73, 125.22, 123.95, 123.82, 121.15, 53.79, 22.20, 21.02, 18.51. HRMS analysis (APCI): calcd for $C_{38}H_{24}F_6$ $(M+H)^+$: 595.1855; found: 595.1845.

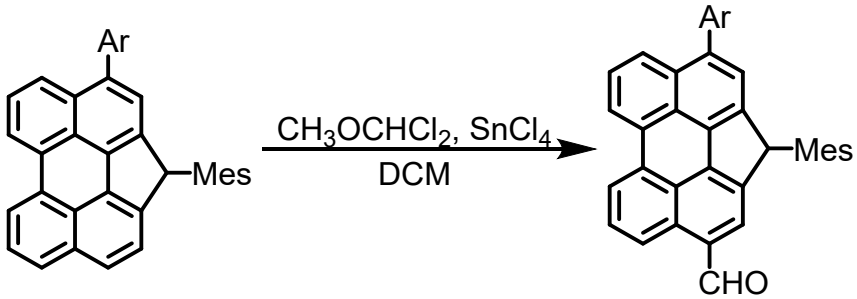

2 **3**

Synthesis of compound **3**: Compound **2** (806 mg, 1.0 mmol) was dissolved in DCM (200 mL) in a round-bottom flask. The solution was cooled in an ice–water bath and purged with nitrogen. $SnCl_4$ (0.35 mL, 3.0 mmol) was added, followed by dropwise addition of Cl_2CHOCH_3 (0.25 mL, 3.0 mmol). The reaction mixture was allowed to warm to room temperature and stirred overnight. The reaction was quenched by the addition of water (10 mL). The organic phase was extracted, and the solvents were removed under reduced pressure. The crude product was purified by column chromatography on silica gel using petroleum ether/DCM (5:1, v/v) as the eluent to afford compound **3** as yellow-green solid (124 mg, 95%). ^{1}H NMR (600 MHz, $CDCl_3$) δ (ppm) = 10.31 (s, 1H), 9.18 (d, *J* = 8.5 Hz, 1H), 8.42 (d, *J* = 7.7 Hz, 2H), 8.08 – 7.91 (m, 4H), 7.87 (t, *J* = 8.0 Hz,

1H), 7.78 – 7.67 (m, 2H), 7.49 (s, 1H), 7.12 (s, 1H), 6.70 (s, 1H), 5.64 (s, 1H), 2.84 (s, 3H), 2.31 (s, 3H), 1.14 (s, 3H). ^{13}C NMR (151 MHz, CDCl3) δ (ppm) = 192.98, 144.24, 142.97, 141.36, 140.24, 138.05, 137.72, 137.41, 135.52, 133.93, 132.28, 132.04, 131.93, 131.50, 131.00, 130.64, 130.58, 130.33, 130.27, 129.69, 129.43, 128.67, 125.73, 125.62, 125.58, 125.07, 124.69, 124.42, 122.61, 122.31, 121.88, 121.50, 53.67, 22.35, 20.98, 18.51. HRMS analysis (APCI): calcd for $C_{39}H_{24}F_6O$ $(M+H)^+$: 623.1804; found: 623.1797.

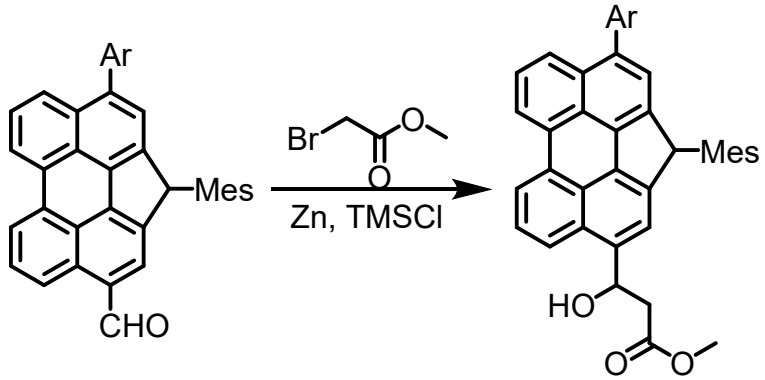

3 **4**

Synthesis of compound **4**: Activated zinc (1.20 g, 18.46 mmol) and TMSCl (0.1 equiv) were placed in a 150 mL double-necked round-bottom flask, and THF (10 mL) was added as the solvent. The mixture was stirred at 0 ℃ under nitrogen atmosphere for 30 min. Methyl bromoacetate (1.8 mL, 19.14 mmol) was then added, and the reaction mixture was stirred at room temperature for 2 h. Subsequently, compound **3** (634 mg, 1.02 mmol) was added, and the mixture was stirred at room temperature for an additional 15 min. The reaction was quenched by the addition of saturated aqueous NH_4Cl (10 mL). The organic layer was extracted and washed successively with saturated aqueous $NaHCO_3$ and saturated aqueous NaCl. After removal of the solvents under reduced pressure, the residue was purified by column chromatography on silica gel using petroleum ether/DCM (3:1, v/v) as the eluent to afford compound **4** as yellowish-brown solid (532 mg, 75%). ^{1}H NMR (600 MHz, $CDCl_3$) δ (ppm) = 8.31 (t, *J* = 7.5 Hz, 2H), 8.09–8.02 (m, 1H), 8.00 (s, 2H), 7.92 (s, 1H), 7.74 – 7.67 (m, 3H), 7.66 – 7.61 (m, 1H), 7.42 (d, *J* = 6.9 Hz, 1H), 7.08 (s, 1H), 6.67 (s, 1H), 5.94 –5.86 (m, 1H), 5.53 (d, *J* = 13.4 Hz, 1H), 3.77 (d, *J* = 14.6 Hz, 3H), 3.22 (d, *J* = 3.2 Hz, 1H), 2.94 (d, *J* = 7.4 Hz, 1H), 2.80 (d, *J* = 3.3 Hz, 3H), 2.64 (s, 1H), 2.30 (d, *J* = 5.1 Hz, 3H), 1.13 (d, *J* = 4.8 Hz, 3H).^{13}C NMR (151 MHz, $CDCl_3$) δ (ppm) = 173.10, 143.54, 141.48, 141.07, 138.31, 137.98, 137.70, 136.95, 136.88, 135.65, 135.19, 132.89, 132.82, 132.12, 131.90, 131.23, 130.49, 130.41, 130.33, 129.47, 128.34, 127.80, 126.01, 125.85, 125.25, 124.17, 123.32, 121.31, 121.19, 120.87, 68.61, 54.00, 52.12, 43.07, 22.17, 20.99, 18.55. HRMS analysis (APCI): calcd for $C_{42}H_{30}F_6O_3$ $(M-H)^-$: 695.2099; found: 695.2017.

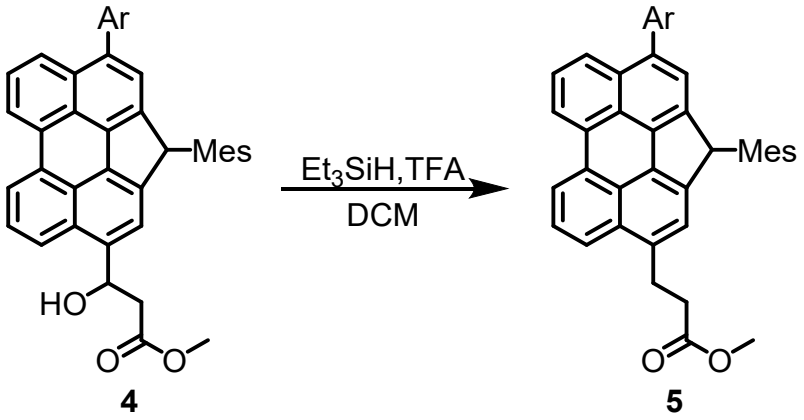

Synthesis of compound **5**: Compound **4** (362 mg, 0.52 mmol) was placed in a 150 mL double-necked round-bottom flask equipped with a magnetic stir bar and dissolved in DCM (40 mL). Et_3SiH (0.90 mL, 5.66 mmol) and TfOH (0.50 mL, 6.26 mmol) were added sequentially to the solution under nitrogen atmosphere. The reaction mixture was stirred at room temperature for 1 h and then quenched by the addition of saturated aqueous Na_2CO_3. The resulting suspension was filtered, and the filtrate was extracted with organic solvent. After removal of the solvents under reduced pressure, the residue was purified by column chromatography on silica gel using petroleum ether/ethyl acetate (20:1, v/v) as the eluent to afford compound **5** as yellowish-brown solid (314.7 mg, 89%). ^{1}H NMR (600 MHz, $CDCl_3$) δ (ppm) = 8.31 (dd, *J* = 7.4, 3.9 Hz, 2H), 8.00 (t, *J* = 4.3 Hz, 3H), 7.91 (s, 1H), 7.74 – 7.66 (m, 2H), 7.63 (t, *J* = 7.9 Hz, 1H), 7.41 (s, 1H), 7.37 (s, 1H), 7.09 (s, 1H), 6.68 (s, 1H), 5.51 (s, 1H), 3.66 (s, 3H), 3.43 (t, *J* = 8.1, 2H), 2.80 (s, 3H), 2.79 – 2.73 (m, 2H), 2.30 (s, 3H), 1.14 (s, 3H). ^{13}C NMR(151 MHz, $CDCl_3$) δ (ppm) = 173.27, 143.45, 141.56, 140.28, 138.16, 137.81, 136.98, 136.74, 136.20, 134.56, 132.82, 132.56, 131.91, 131.68, 131.51, 131.10, 130.50, 130.24, 130.14, 129.28, 128.13, 127.42, 125.84, 125.67, 125.06, 124.46, 124.34, 123.81, 123.56, 123.40, 122.53, 121.03, 120.95, 53.66, 51.59, 35.73, 31.43, 30.23, 29.69, 28.98, 21.99, 20.84, 18.36. HRMS analysis (APCI): calcd for $C_{42}H_{30}F_6O_2$ $(M+H)^+$: 681.2223; found: 681.2213.

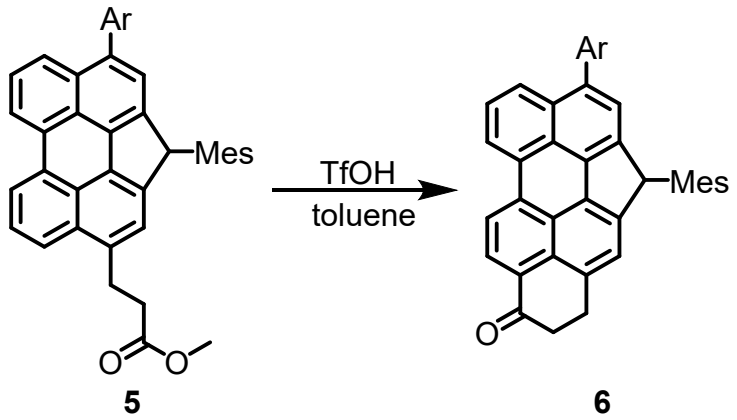

Synthesis of compound **6**: Compound **5** (211 mg, 0.31 mmol) and toluene (100 mL) were placed in a 250 mL double-necked round-bottom flask. TfOH (0.369 mL, 4.62 mmol) was added dropwise under a nitrogen atmosphere. The reaction mixture was heated at 90 °C for 5 h and then

cooled to room temperature. Water was added, and the organic materials were extracted. The combined organic layers were washed successively with saturated aqueous $NaHCO_3$ and saturated aqueous NaCl. After removal of the solvents under reduced pressure, the residue was purified by column chromatography on silica gel using petroleum ether/DCM (2:1, v/v) as the eluent to afford compound **6** as a light green solid (176.77 mg, 88%).^{1}H NMR (600 MHz, $CDCl_3$) δ (ppm) = 8.37 (d, *J* = 7.4 Hz, 1H), 8.33 (d, *J* = 7.8 Hz, 1H), 8.26 (d, *J* = 7.8 Hz, 1H), 8.00 (s, 2H), 7.93 (s, 1H), 7.77 (d, *J* = 8.4 Hz, 1H), 7.68 (t, *J* = 7.9 Hz, 1H), 7.46 (d, *J* = 6.4 Hz, 2H), 7.11 (s, 1H), 6.71 (s, 1H), 5.57 (s, 1H), 3.46 (p, *J* = 8.3 Hz, 2H), 3.03 (t, *J* = 7.1 Hz, 2H), 2.82 (s, 3H), 2.31 (s, 3H), 1.15 (s, 3H).^{13}C NMR (151 MHz, $CDCl_3$) δ (ppm) = 197.73, 143.30, 142.03, 141.39, 138.22, 137.95, 137.37, 137.14, 136.55, 135.32, 134.08, 132.62, 132.20, 131.97, 131.56, 131.25, 130.99, 130.49, 130.27, 130.19, 129.55, 128.97, 128.85, 128.33, 125.87, 125.57, 125.41, 122.69, 122.55, 120.94, 54.19, 39.15, 31.67, 29.39, 18.52. HRMS analysis (APCI): calcd for $C_{41}H_{26}F_6O$ $(M+H)^+$: 649.1961; found: 649.1952.

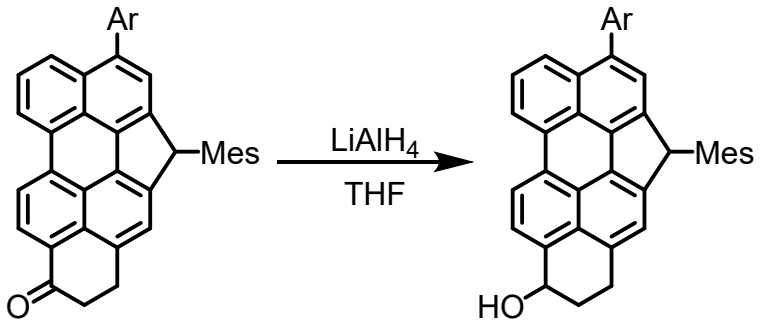

6 **7**

Synthesis of compound **7**: Compound **6** (97.2 mg, 0.15 mmol) was placed in a 100 mL double-necked round-bottom flask and dissolved in THF (10 mL). The solution was degassed by freeze–pump–thaw cycles using liquid nitrogen and backfilled with nitrogen. $LiAlH_4$ (8.77 mg, 0.23 mmol) was added under a nitrogen atmosphere, and the reaction mixture was stirred at 0 °C for 20 min. The reaction mixture was then poured into ice–water, and the organic materials were extracted. The combined organic layers were washed successively with saturated aqueous $NaHCO_3$ and saturated aqueous NaCl. After removal of the solvents under reduced pressure, the residue was purified by column chromatography on silica gel using petroleum ether/ethyl acetate (2:1, v/v) as the eluent to afford compound **7** as pale green solid (82.88 mg, 85%). ^{1}H NMR (600 MHz, $CDCl_3$) δ (ppm) = 8.22 (d, *J* = 7.6 Hz, 2H), 8.01 (d, *J* = 5.0 Hz, 2H), 7.92 (s, 1H), 7.67 (d, *J* = 3.8 Hz, 2H), 7.63–7.57 (m, 1H), 7.40 (d, *J* = 5.6 Hz, 1H), 7.30 (s, 1H), 7.10 (s, 1H), 6.69 (s, 1H), 5.49 (d, *J* = 6.9 Hz, 1H), 5.16 (dt, *J* = 8.3, 4.4 Hz, 1H), 3.36 – 3.22 (m, 1H), 3.18 – 3.05 (m, 1H), 2.80 (s, 3H), 2.31 (s, 3H), 2.22 (m, 1H), 1.15 (d, *J* = 3.2 Hz, 3H). ^{13}C NMR (151 MHz, $CDCl_3$) δ (ppm) = 143.69, 141.97, 140.28, 138.37, 138.33, 138.16, 138.04, 137.95, 137.30, 136.88, 135.08, 134.51, 134.01, 132.99, 132.09, 131.87, 131.75, 131.70, 131.40, 130.84, 130.40, 130.29, 128.52, 128.26, 126.00, 125.27, 124.52, 124.34, 124.23, 123.82, 123.79, 122.71, 121.64, 121.27, 120.97, 120.86, 120.84, 69.13, 69.04, 53.93, 22.11, 20.99, 18.56. HRMS analysis (APCI): calcd for $C_{41}H_{28}F_6O$ $(M-H)^-$: 649.1971; found: 649.1960.

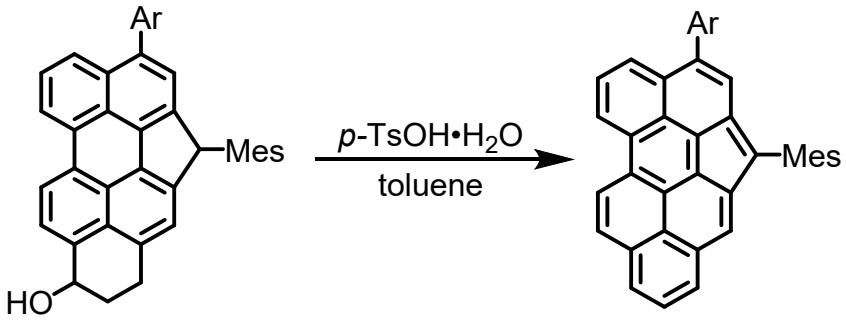

7 **Pery-56**

Synthesis of compound **Pery-56**: Compound **7** (78 mg, 0.12 mmol) was dissolved in toluene (10 mL) in a round-bottom flask under a nitrogen atmosphere. A catalytic amount of *p*-TsOH·H_2O was added to the solution. The reaction mixture was degassed by freeze–pump–thaw cycles using liquid nitrogen and then heated to 90 ℃ for 5 min. After cooling to room temperature, the mixture was vacuum filtered to remove the solid catalyst. The resulting mixture was purified by column chromatography on silica gel using petroleum ether/DCM (10:1, v/v) as the eluent to afford compound **Pery-56** as a green solid (68 mg, 90%). ^{1}H NMR (600 MHz, $CDCl_3$) δ (ppm) = 8.92 (d, *J* = 9.0 Hz, 1H), 8.78 (d, *J* = 8.4 Hz, 1H), 8.46 (d, *J* = 7.8 Hz, 1H), 8.42 (d, *J* = 7.4 Hz, 1H), 8.34 (s, 1H), 8.30 (d, *J* = 9.1 Hz, 1H), 8.12 – 8.06 (m, 1H), 8.05 (s, 2H), 7.94 (s, 1H), 7.67 (t, *J* = 8.0 Hz, 1H), 7.45 (d, *J* = 7.3 Hz, 1H), 7.10 (s, 2H), 6.90 (s, 1H), 2.42 (s, 3H), 2.33 (s, 6H). ^{13}C NMR (151 MHz, $CDCl_3$) δ (ppm) = 143.12, 140.88, 140.78, 138.19, 137.81, 137.46, 133.33, 132.61, 132.45, 132.10, 131.88, 131.67, 131.57, 131.45, 130.24, 130.14, 129.92, 129.57, 128.62, 128.35, 127.53, 127.18, 126.49, 126.23, 126.14, 125.36, 124.75, 124.47, 123.85, 122.67, 122.54, 121.78, 121.55, 120.56, 21.41, 21.35. HRMS analysis (APCI): calcd for $C_{41}H_{24}F_6$ $(M+H)^+$: 631.1855; found: 631.1844.

2. Photoelectrical Properties

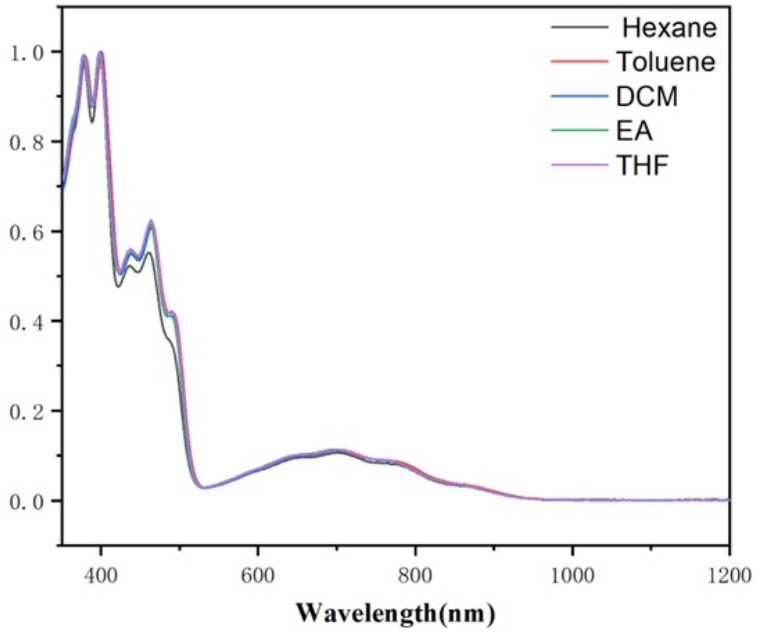

Figure S1. UV-Vis-NIR spectrum of **Pery-56** in various solvents.

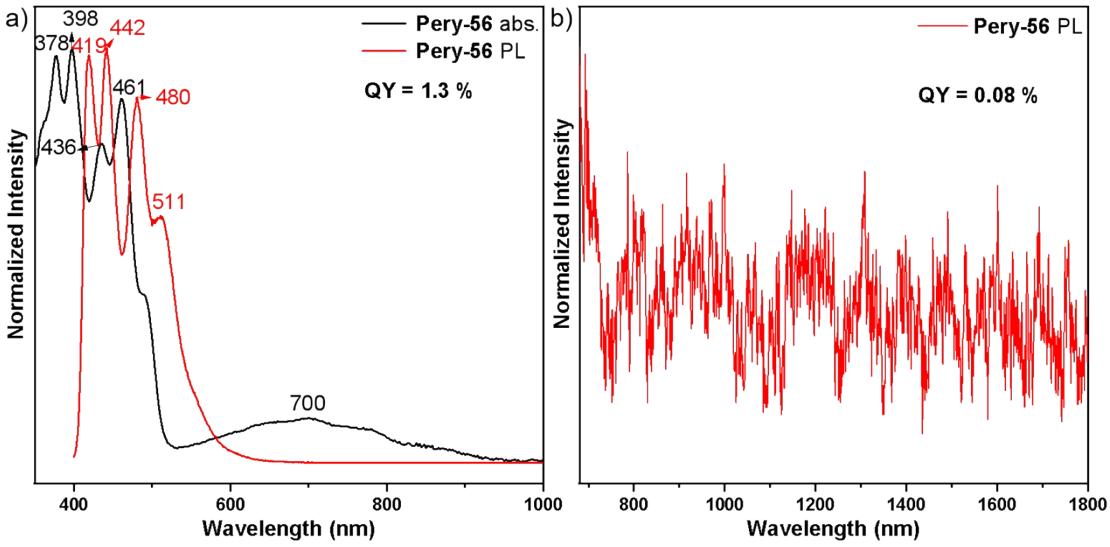

Figure S2. a) UV-Vis-NIR absorption and emission (λ_{ex} = 390 nm) spectra of **Pery-56** in dichloromethane; b) Emission (λ_{ex} = 700 nm) spectra of **Pery-56** in dichloromethane.

3. Crystal Information

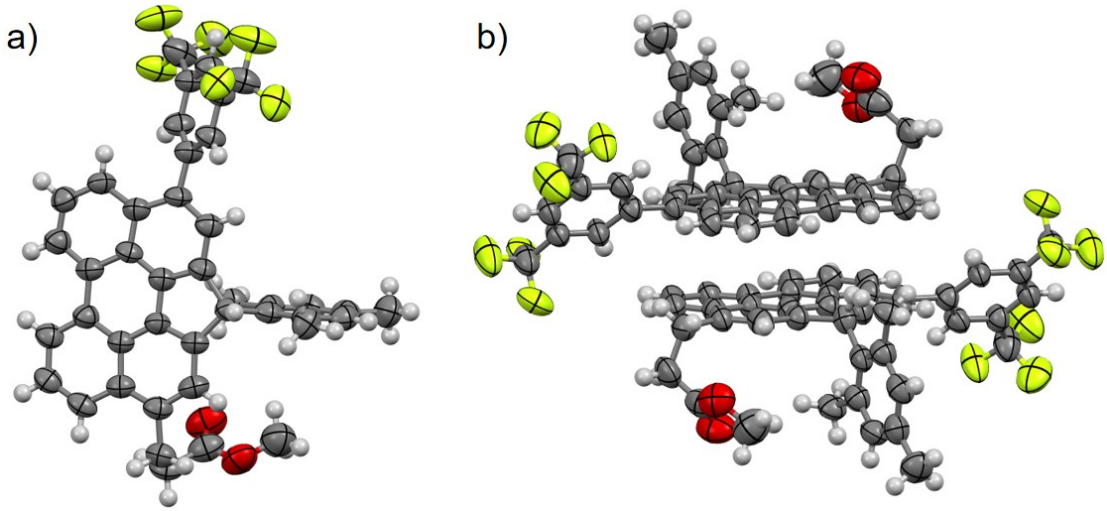

Figure S3. a) The thermal ellipsoid (50%) structure of **5**; b) The packing mode of single crystal **5** in the unit cell.

Table S1. Crystallographic data for **5**.

Identification code	**5**
Empirical formula	$C_{42}H_{30}F_6O_2$
Formula weight	680.66
Temperature	193.00 K
Crystal system	monoclinic
Space group	$C2_{/c}$
a	29.26(3) Å
b	9.061(7) Å
c	29.39(3) Å
α	90°
β	113.23(3)°
γ	90°
Volume	7160(11) $Å^3$
Z	8
Density (calculated)	1.263 g/cm^3
Absorption coefficient	0.526 mm^{-1}
F(000)	2816.0
Crystal size	0.12 × 0.11 × 0.09 mm^3
Radiation	GaKα (λ = 1.34139)
Theta range for data collection	14.11 to 105.962°
Index ranges	$-34 \le h \le 34$, $-10 \le k \le 10$, $-34 \le l \le 34$
Reflections collected	19306

Independent reflections	6301 [R_{int} = 0.1510, R_{sigma} = 0.1876]
Data/restraints/parameters	6301/240/530
Goodness-of-fit on F^2	0.998
Final R indexes [I>=2σ (I)]	R_1 = 0.0993, wR_2 = 0.2422
Final R indexes [all data]	R_1 = 0.2402, wR_2 = 0.3208
Largest diff. peak/hole	0.24/-0.25 eÅ^{-3}

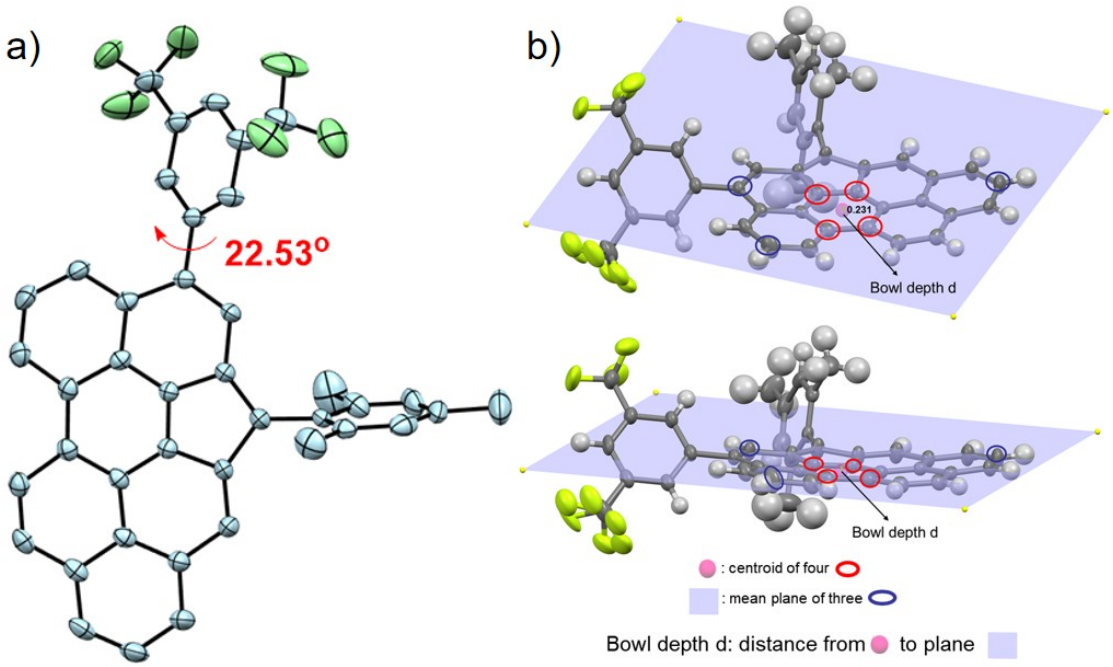

Figure S4. a) The thermal ellipsoid (50%) structure of **Pery-56**; b) Bowl depth of **Pery-56**.

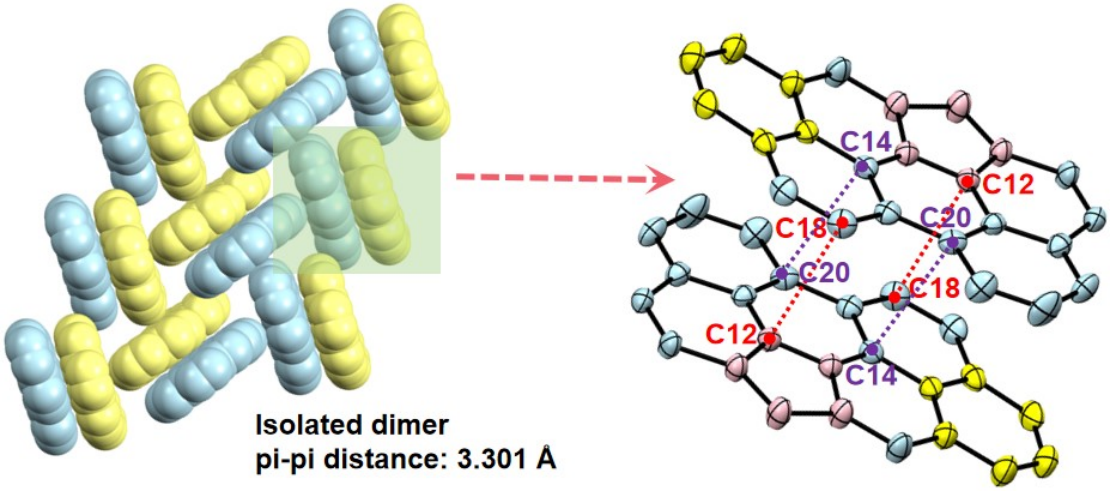

Figure S5. The packing mode of single crystal **Pery-56** in the unit cell.

Table S2. Crystallographic data for **Pery-56**.

Identification code	**Pery-56**
Empirical formula	$C_{41}H_{24}F_6$
Formula weight	630.60
Temperature	193.00 K
Crystal system	monoclinic
Space group	$P2_{1/c}$
a	18.9255(4) Å
b	10.0582(2) Å
c	16.7712(4) Å
α	90°
β	108.7590(10)°
γ	90°
Volume	3022.92(11) $Å^3$
Z	4
Density (calculated)	1.386 g/cm^3
Absorption coefficient	0.885 mm^{-1}
F(000)	1296.0
Crystal size	0.13 × 0.11 × 0.08 mm^3
Radiation	CuKα (λ = 1.54178)
Theta range for data collection	4.932 to 149.092°
Index ranges	$-22 \leq h \leq 23$, $-10 \leq k \leq 12$, $-20 \leq l \leq 20$
Reflections collected	23454
Independent reflections	5950 [R_{int} = 0.0653, R_{sigma} = 0.0580]
Data/restraints/parameters	5950/420/464
Goodness-of-fit on F^2	1.095
Final R indexes [I>=2σ (I)]	R_1 = 0.0794, wR_2 = 0.2054
Final R indexes [all data]	R_1 = 0.1025, wR_2 = 0.2177
Largest diff. peak/hole	0.70/-0.39 $eÅ^{-3}$

4. DFT Calculations

Theoretical calculations were performed using the Gaussian 16 software package and Multiwfn program.[1][2][3] Unless stated otherwise, geometry optimizations of all molecules in the ground state (S_0) were performed using the B3LYP/6-31(d,p).[4] The simulated electronic absorption spectra are on the basis of the optimized ground-state geometry and wavefunction by time-dependent density functional theory (TD-DFT) calculation at PBE0/6-311(d,p) level.[5] Nucleus independent chemical shifts (NICS)[6] values and anisotropy of the induced current density (ACID)[7] plot for the simulated aromatic properties of studied molecules have been computed at the B3LYP/6-311(d,p) level based on the optimized ground-state geometries. Electrostatic potential (ESP) on the basis of the geometry and wavefunction at B3LYP/6-31(d,p) level were performed with the Multiwfn 3.8 (dev) code. Isosurface maps of various real space functions were rendered by means of Visual Molecular Dynamics (VMD) software based on the files exported by Multiwfn.[3][8]

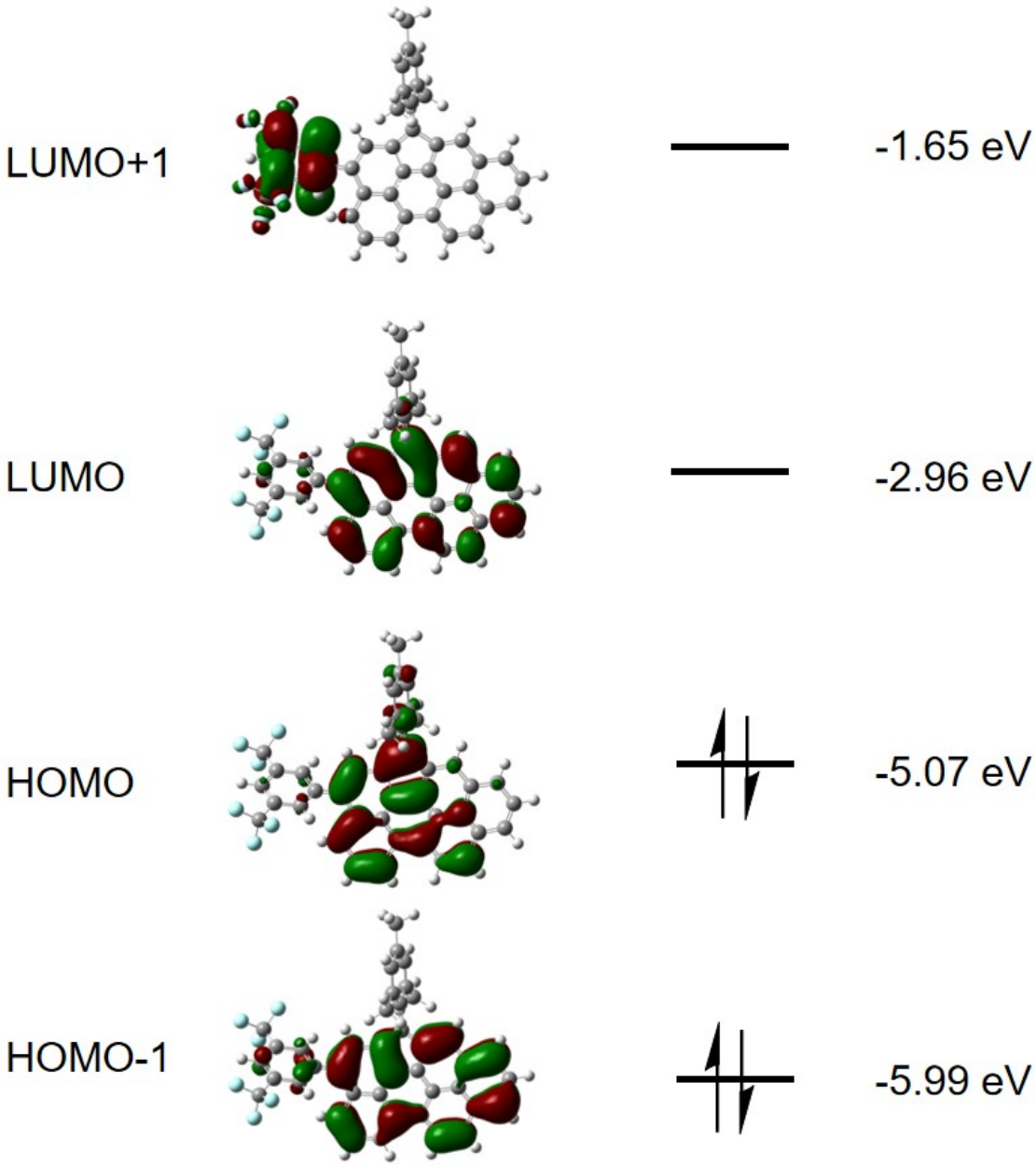

Figure S6. HOMO-1, HOMO, LUMO and LUMO+1 orbitals and their energy levels of **Pery-56**, calculated at B3LYP/6-31G(d,p).

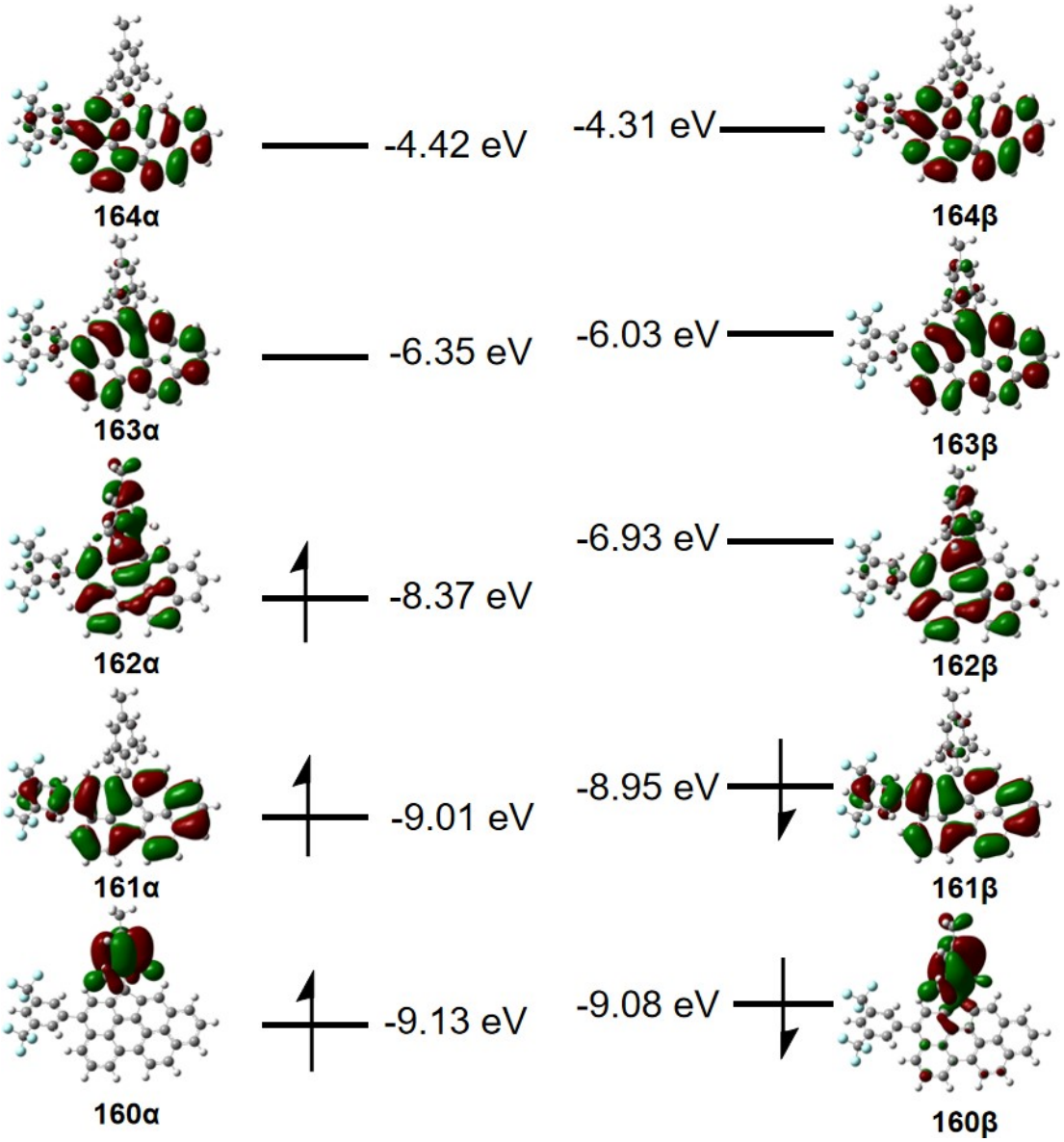

Figure S7. The frontier molecular orbital profiles and energy diagram of **Pery-56**$^{+\bullet}$ obtained by calculation at the B3LYP/6-31G(d,p) level.

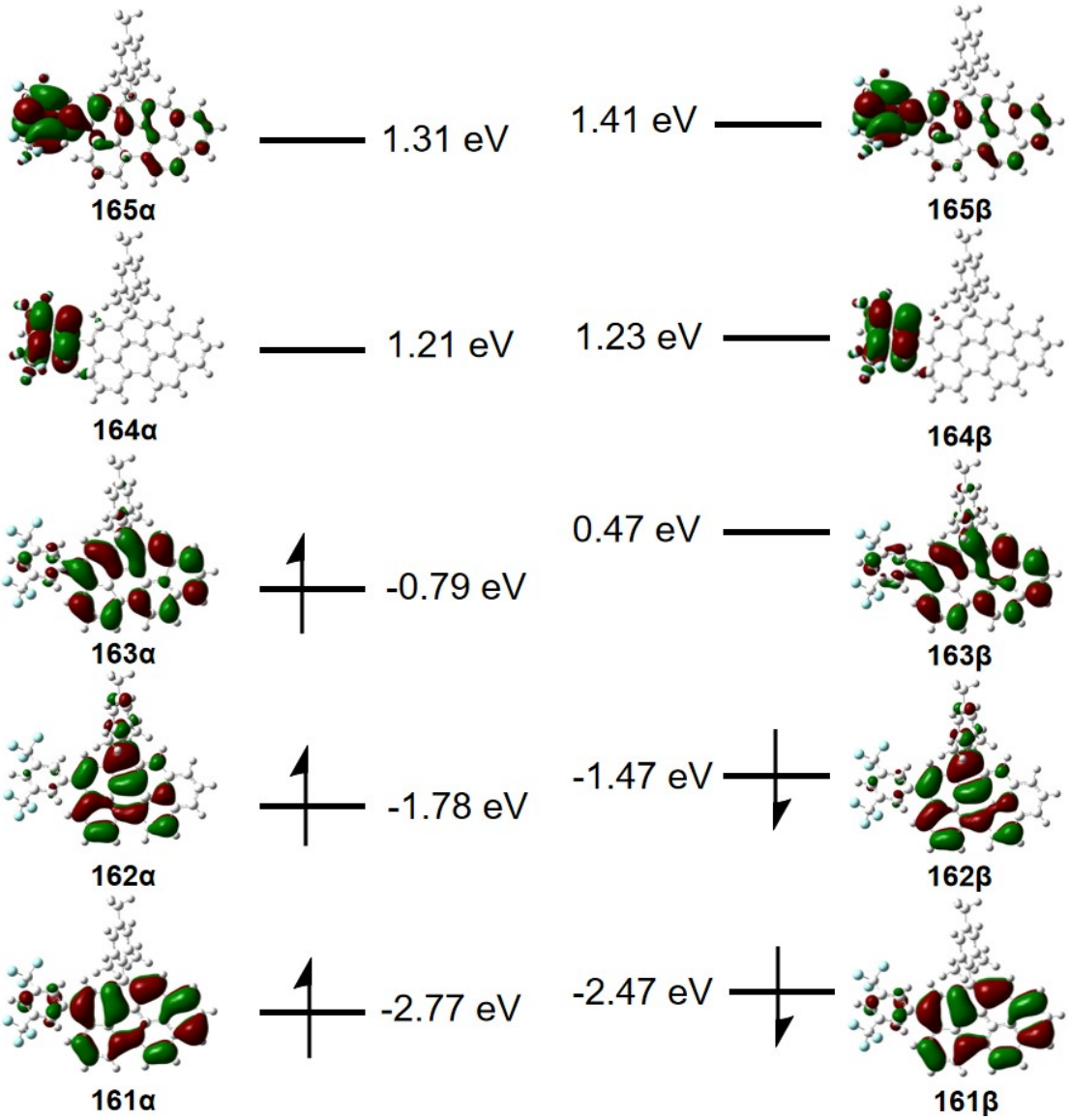

Figure S8. The frontier molecular orbital profiles and energy diagram of **Pery-56**$^{-\bullet}$ obtained by calculation at the B3LYP/6-31G(d,p) level.

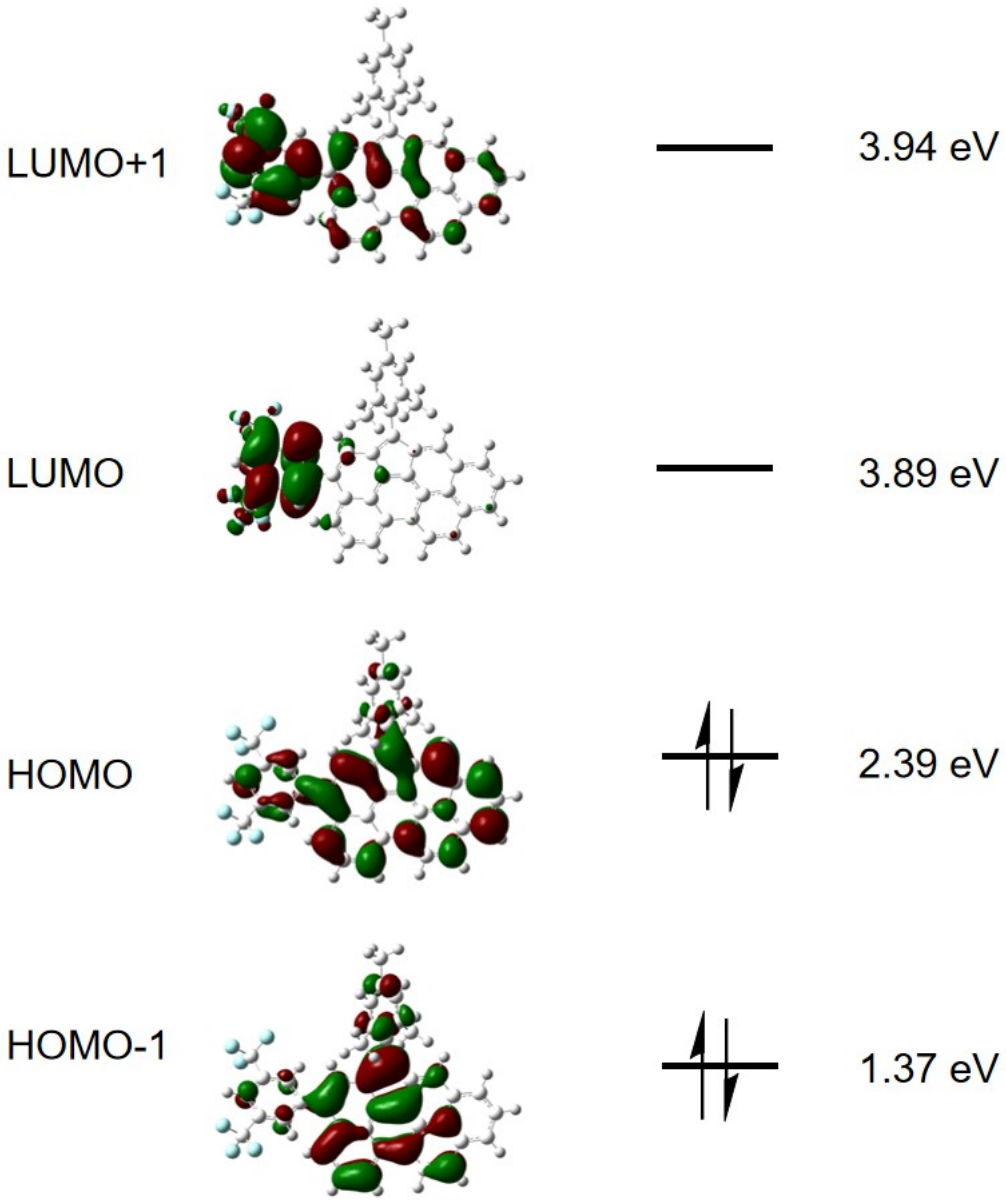

Figure S9. The frontier molecular orbital profiles and energy diagram of **Pery-56**$^{2-}$ obtained by calculation at the B3LYP/6-31G(d,p) level.

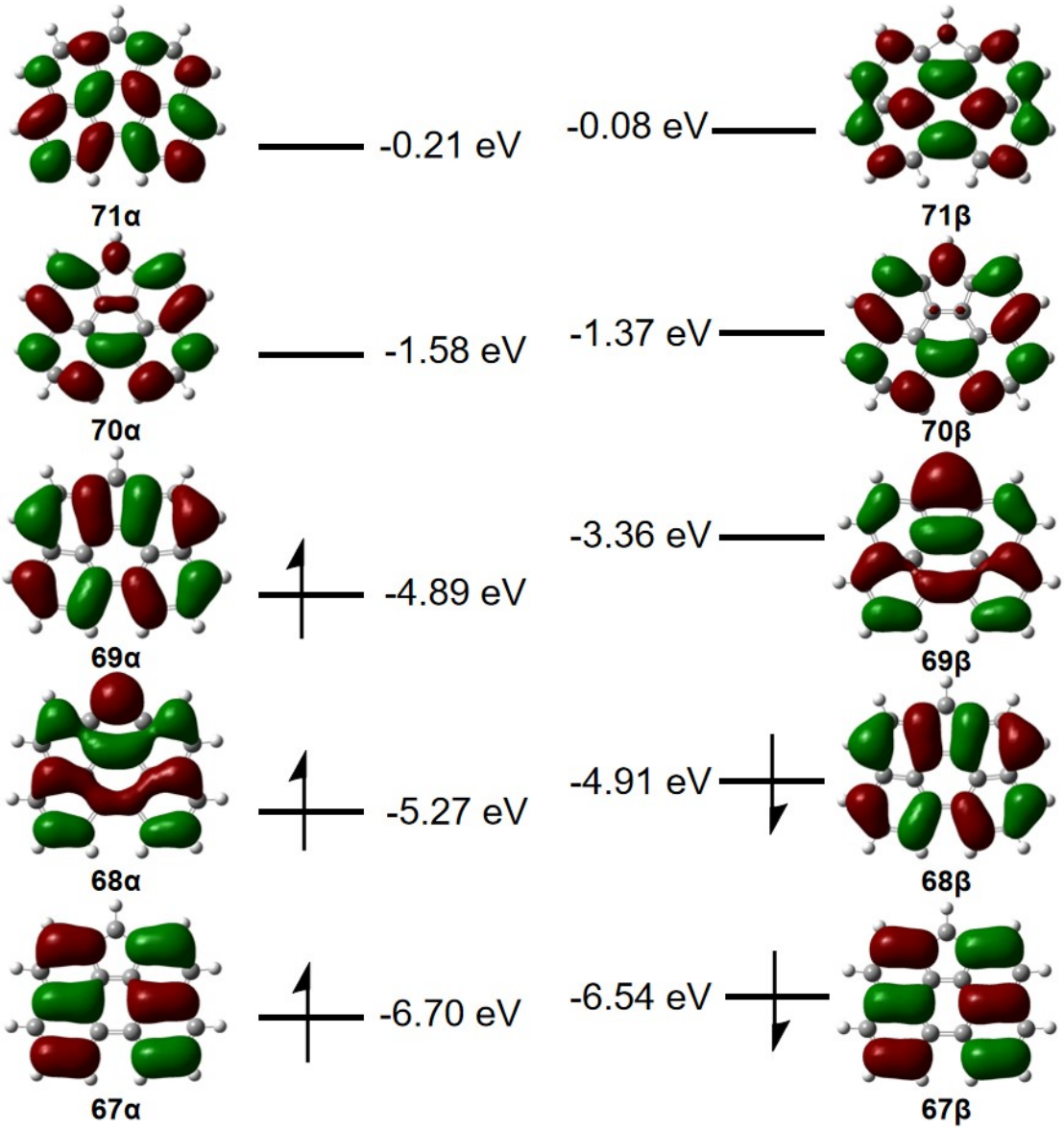

Figure S10. The frontier molecular orbital profiles and energy diagram of **only five-membered rings at the bay region** obtained by calculation at the B3LYP/6-31G(d,p) level.

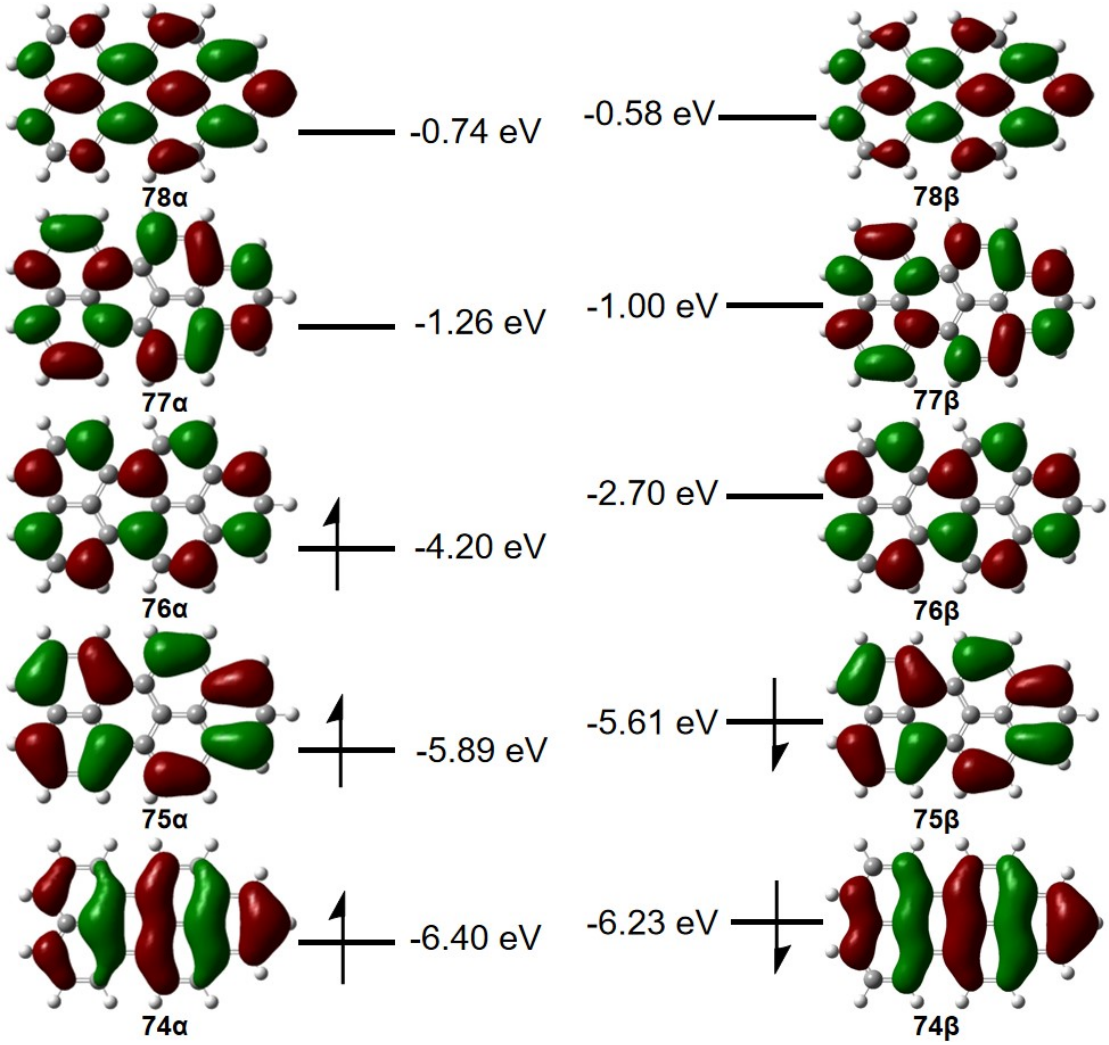

Figure S11. The frontier molecular orbital profiles and energy diagram of **only six-membered rings at the peri position** obtained by calculation at the B3LYP/6-31G(d,p) level.

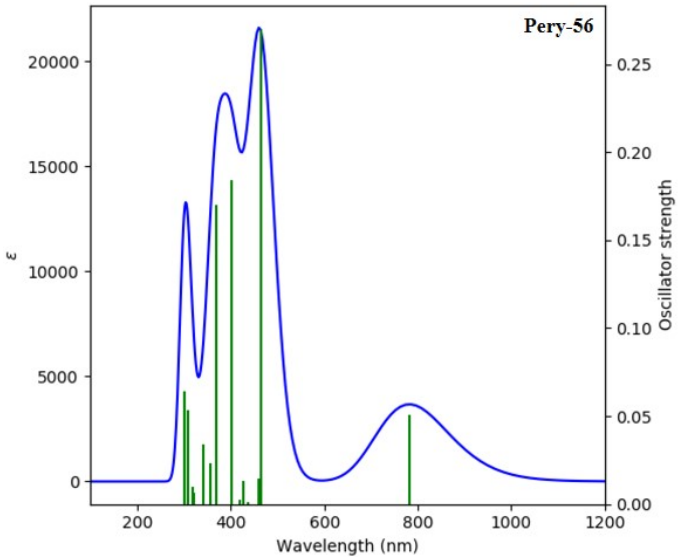

Figure S12. TD-DFT (PBE0/6-311G(d,p)) simulated UV/Vis absorption spectra with oscillator strength of compound **Pery-56**.

Table S3. The selected wavelength, oscillator strength, and compositions of major electronic transitions of **Pery-56** calculated by TD-DFT (B3LYP /6-311G(d,p)).

	State	Energy [eV]	λ [nm]	*f*	Orbitals(coefficient)
Pery-56	S1	1.59	782	0.0507	HOMO→LUMO (98%)
	S2	2.67	464	0.2701	H-1→LUMO (80%)
	S3	2.70	459	0.0143	H-2→LUMO (95%)
	S4	2.84	436	0.0012	H-3→LUMO (99%)
	S5	2.91	427	0.013	H-4→LUMO (60%), HOMO→L+1 (15%), HOMO→L+3 (18%)
	S6	2.96	420	0.0024	H-4→LUMO (10%), HOMO→L+1 (82%)
	S7	3.08	403	0.184	HOMO→L+2 (82%)
	S8	3.35	370	0.1703	H-4→LUMO (16%), HOMO→L+3 (67%)
	S9	3.48	356	0.023	H-5→LUMO (93%)
	S10	3.63	342	0.0343	HOMO→L+4 (91%)
	S11	3.87	320	0.0063	H-1→L+1 (94%)
	S12	3.90	318	0.0097	H-6→LUMO (65%), H-1→L+2 (20%)
	S13	4.03	308	0.0532	H-1→L+2 (57%), H-1→L+3 (18%)
	S14	4.10	302	0.0644	H-8→LUMO (11%), H-1→L+3 (35%), HOMO→L+5 (10%), HOMO→L+6 (12%)
	S15	4.16	301	0.0634	H-7→LUMO (21%), H-1→L+3 (18%), HOMO→L+5 (14%), HOMO→L+6 (26%)

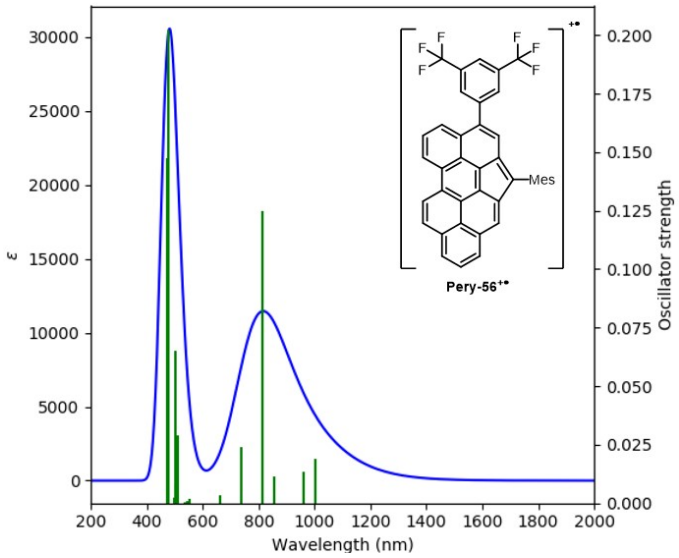

Figure S13. TD-DFT (PBE0/6-311G(d,p)) simulated UV/Vis absorption spectra with oscillator strength of compound **Pery-56**$^{+\bullet}$.

Table S4. The selected wavelength, oscillator strength, and compositions of major electronic transitions of **Pery-56**$^{+\bullet}$ calculated by TD-DFT (B3LYP /6-311G(d,p)) .

	State	Energy [eV]	λ [nm]	*f*	Orbitals(coefficient)
Pery-56$^{+\bullet}$	S1	1.24	1004	0.0189	HOMO(α)→LUMO(α) (13%)，HOMO(β)→LUMO(β) (78%)
	S2	1.29	959	0.0134	HOMO(α)→LUMO(α) (79%)，HOMO(β)→LUMO(β) (12%)
	S3	1.45	856	0.0115	H-2(β)→LUMO(β) (18%) H-1(β)→LUMO(β) (78%)
	S4	1.52	814	0.1249	H-2(β)→LUMO(β) (74%) H-1(β)→LUMO(β) (14%)
	S5	1.68	736	0.0242	H-1(α)→LUMO(α) (50%), HOMO(β)→L+1(β) (35%)
	S6	1.87	663	0.0036	H-3(β)→LUMO(β) (90%)
	S7	2.25	550	0.0018	H-2(α)→LUMO(α) (88%)
	S8	2.29	542	0.0007	H-3(α)→LUMO(α) (55%), H-2(β)→L+1(β) (12%), H-1(β)→L+1(β) (10%)
	S9	2.32	535	0.0004	H-6(β)→LUMO(β) (50%), H-4(β)→LUMO(β) (28%)
	S10	2.43	511	0.0291	H-4(α)→LUMO(α) (48%), H-3(α)→LUMO(α) (17%)
	S11	2.47	503	0.0649	H-6(β)→LUMO(β) (13%), H-4(β)→LUMO(β) (54%)

	S12	2.47	502	0.0085	H-3(α)→LUMO(α) (10%), H-4(β)→LUMO(β) (10%), H-1(β)→L+1(β) (49%)
	S13	2.50	496	0.0022	H-2(β)→L+1(β) (70%), H-1(β)→L+1(β) (19%)
	S14	2.60	477	0.2023	H-1(α)→LUMO(α) (15%), H-5(β)→LUMO(β) (50%), HOMO(β)→L+1(β) (20%)
	S15	2.62	474	0.1475	H-1(α)→LUMO(α) (12%), H-6(β)→LUMO(β) (17%), H-5(β)→LUMO(β) (42%), HOMO(β)→L+1(β) (14%)

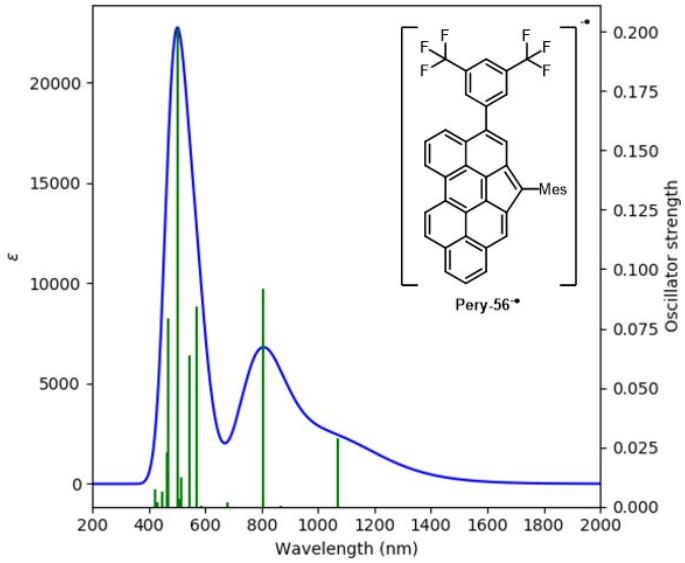

Figure S14. TD-DFT (PBE0/6-311G(d,p)) simulated UV/Vis absorption spectra with oscillator strength of compound **Pery-56**$^{-\bullet}$.

Table S5. The selected wavelength, oscillator strength, and compositions of major electronic transitions of **Pery-56**$^{-\bullet}$ calculated by TD-DFT (B3LYP /6-311G(d,p)).

	State	Energy [eV]	λ [nm]	*f*	Orbitals(coefficient)
Pery-56$^{-\bullet}$	S1	1.16	1069	0.0289	HOMO(β)→LUMO(β) (96%)
	S2	1.43	868	0.0003	HOMO(α)→LUMO(α) (98%)
	S3	1.54	803	0.0919	HOMO(α)→L+1(α) (90%)
	S4	1.83	677	0.0019	HOMO(α)→L+2(α) (76%), H-1(β)→LUMO(β) (15%)
	S5	2.11	587	0.0002	HOMO(β)→L+1(β) (98%)

S6	2.18	570	0.0841	H-1(α)→L+1(α) (24%), HOMO(β)→L+2(β) (58%)
S7	2.28	545	0.064	HOMO(α)→L+3(α) (24%), H-1(β)→LUMO(β) (43%), HOMO(β)→L+2(β) (16%)
S8	2.40	516	0.0121	H-1(α)→L+1(α) (17%), HOMO(α)→L+3(α) (59%)
S9	2.43	511	0.0035	H-1(α)→LUMO(α) (97%)
S10	2.48	500	0.2013	H-1(α)→L+1(α) (36%), H-1(β)→LUMO(β) (15%), HOMO(β)→L+2(β) (14%)
S11	2.65	468	0.0794	H-1(α)→L+1(α) (13%), H-1(α)→L+2(α) (17%), HOMO(α)→L+4(α) (26%), HOMO(β)→L+3(β) (27%)
S12	2.67	465	0.0226	H-1(α)→L+2(α) (10%), HOMO(α)→L+4(α) (64%), HOMO(β)→L+3(β) (17%)
S13	2.78	447	0.0066	HOMO(α)→L+5(α) (27%), HOMO(α)→L+6(α) (27%), H-2(β)→LUMO(β) (34%)
S14	2.87	432	0.0017	HOMO(α)→L+5(α) (23%), H-2(β)→LUMO(β) (30%), HOMO(β)→L+3(β) (12%)
S15	2.93	423	0.0074	HOMO(α)→L+5(α) (45%), HOMO(α)→L+6(α) (31%)

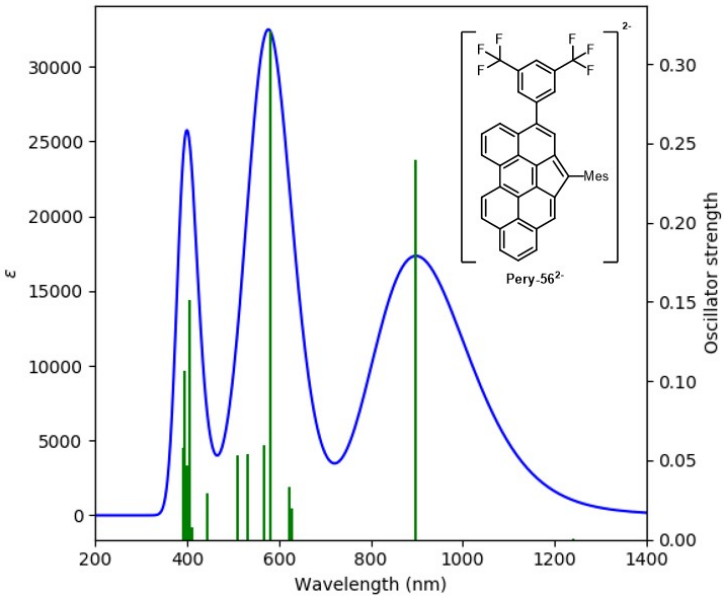

Figure S15. TD-DFT (PBE0/6-311G(d,p)) simulated UV/Vis absorption spectra with oscillator strength of compound **Pery-56^{2-}**.

Table S6. The selected wavelength, oscillator strength, and compositions of major electronic transitions of **Pery-56^{2-}** calculated by TD-DFT (B3LYP /6-311G(d,p)).

	State	Energy [eV]	λ [nm]	*f*	Orbitals(coefficient)
Pery-56^{2-}	S1	1.00	1240	0.0008	HOMO→LUMO (77%), HOMO→L+1 (22%)
	S2	1.38	898	0.2393	HOMO→LUMO (21%), HOMO→L+1 (74%)
	S3	1.97	629	0.0198	H-1→LUMO (27%), HOMO→L+2 (64%)
	S4	2.00	621	0.0331	H-1→LUMO (68%), H-1→L+1 (11%), HOMO→L+2 (18%)
	S5	2.13	581	0.321	H-1→L+1 (82%)
	S6	2.18	569	0.0596	HOMO→L+3 (90%)
	S7	2.33	532	0.054	HOMO→L+4 (91%)
	S8	2.43	511	0.0529	HOMO→L+5 (87%)
	S9	2.79	445	0.0005	HOMO→L+6 (98%)
	S10	2.80	443	0.0293	H-1→L+2 (70%), HOMO→L+7 (23%)
	S11	3.01	412	0.0076	H-2→LUMO (87%)
	S12	3.05	406	0.1514	H-2→L+1 (16%), H-1→L+2 (15%), HOMO→L+7 (55%)
	S13	3.11	399	0.0465	H-2→L+1 (15%), H-1→L+3 (43%), HOMO→L+8 (34%)
	S14	3.15	393	0.1068	H-2→L+1 (53%), H-1→L+3 (16%)
	S15	3.18	390	0.0579	H-1→L+3 (31%), HOMO→L+8 (49%)

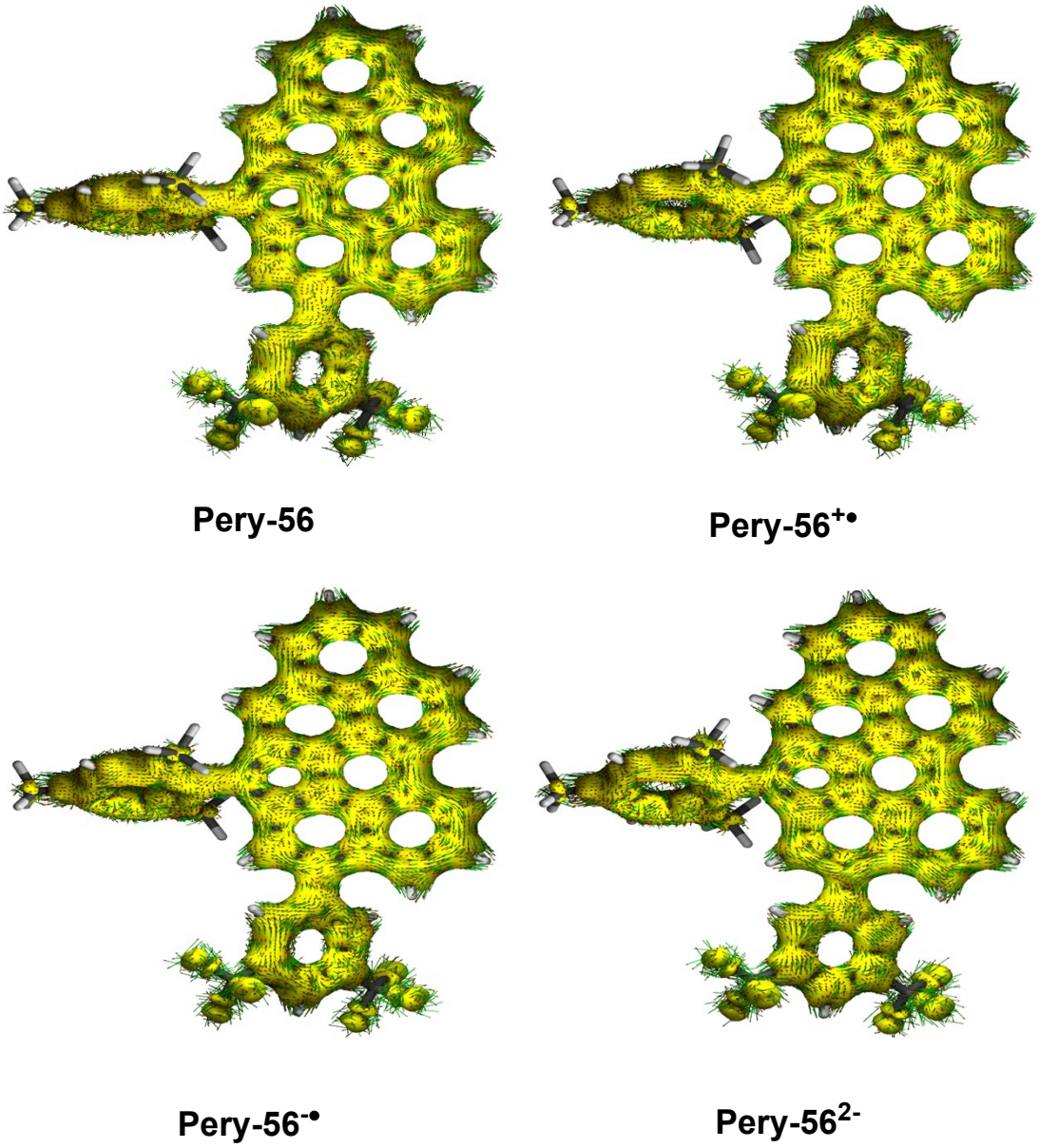

Figure S16. Calculated ACID plots including π and σ electrons contribution of **Pery-56**, **Pery-56$^{+\bullet}$**, **Pery-56$^{-\bullet}$** and **Pery-56^{2-}** (iso-value = 0.05).

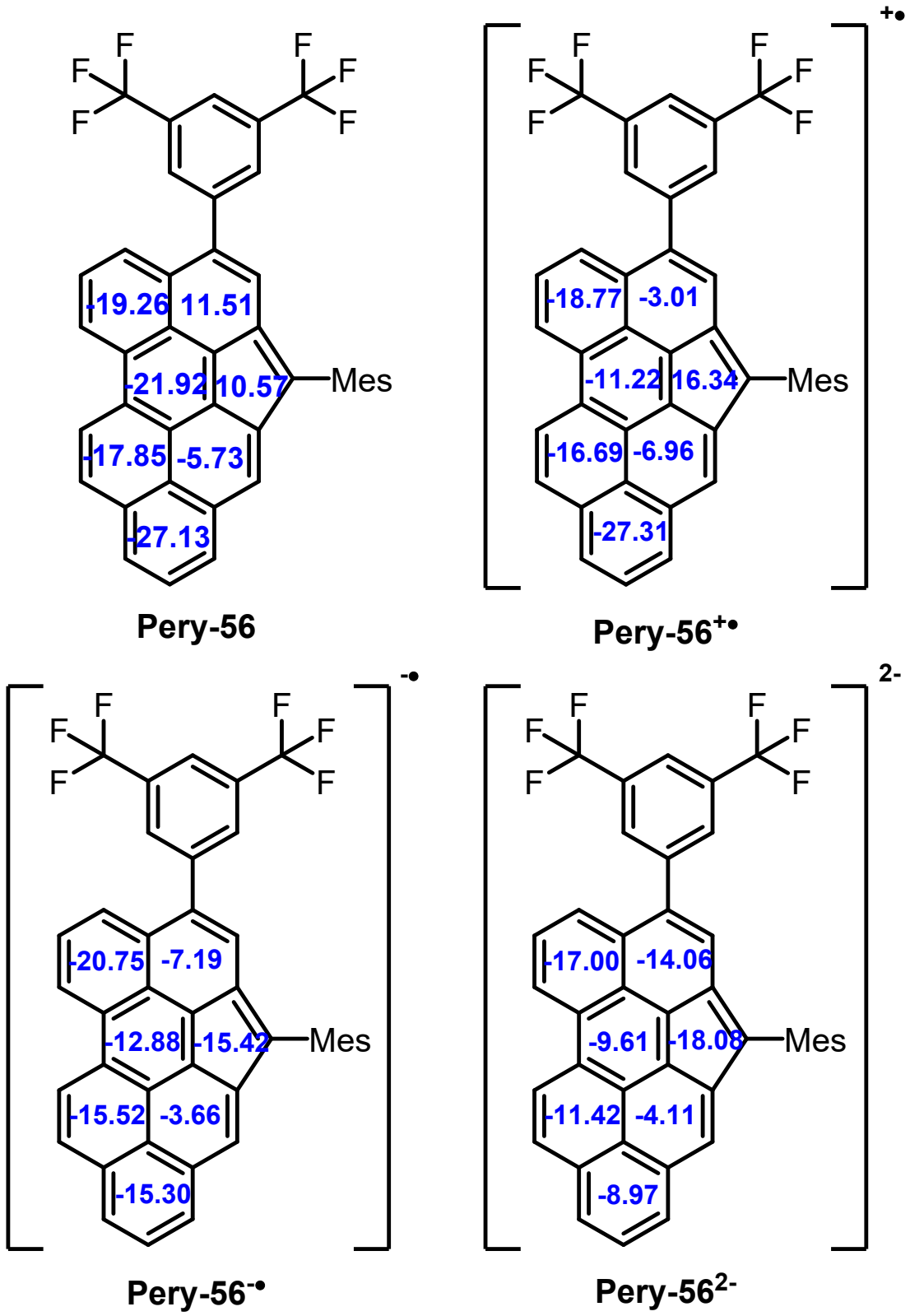

Figure S17. NICS(1)$_{zz}$ plots of **Pery-56**, **Pery-56**$^{+\bullet}$, **Pery-56**$^{-\bullet}$ and **Pery-56**$^{2-}$calculated at B3LYP/6-311G(d,p).

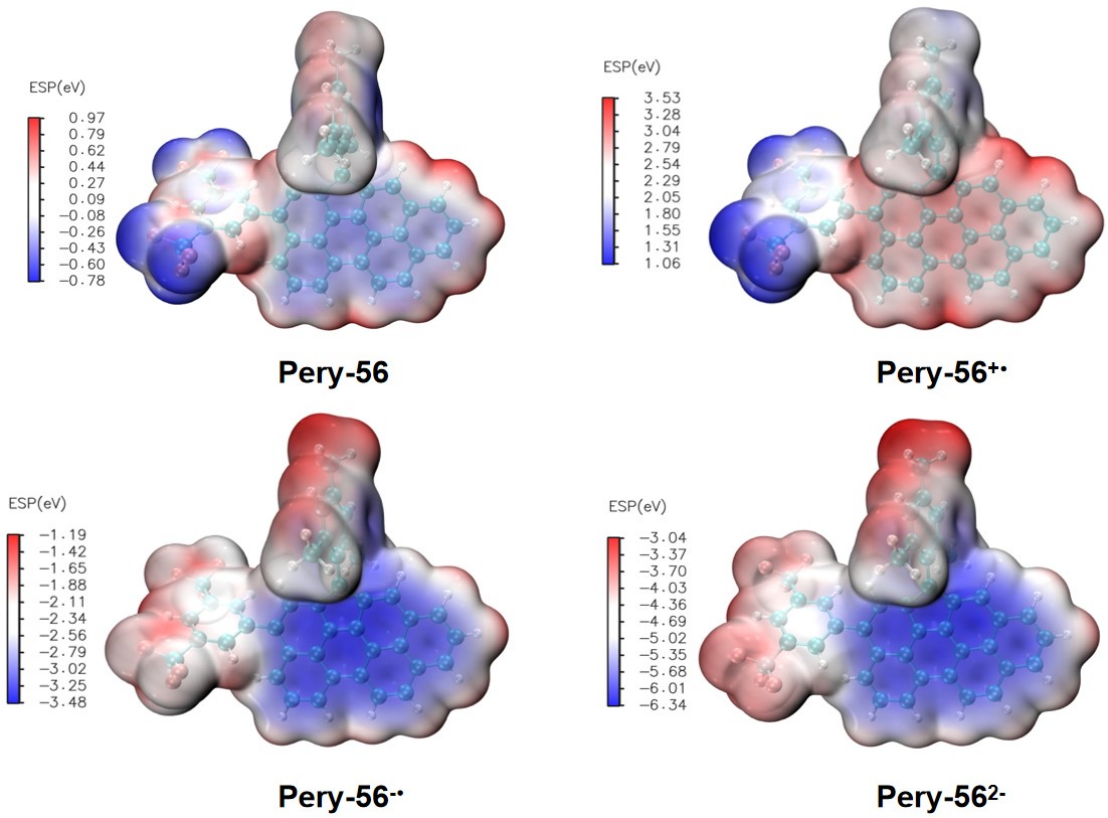

Figure S18. ESP plots of **Pery-56**, **Pery-56$^{+\bullet}$**, **Pery-56$^{-\bullet}$** and **Pery-56^{2-}**calculated at B3LYP/6-311G(d,p).

5. NMR and HR-MS Spectra

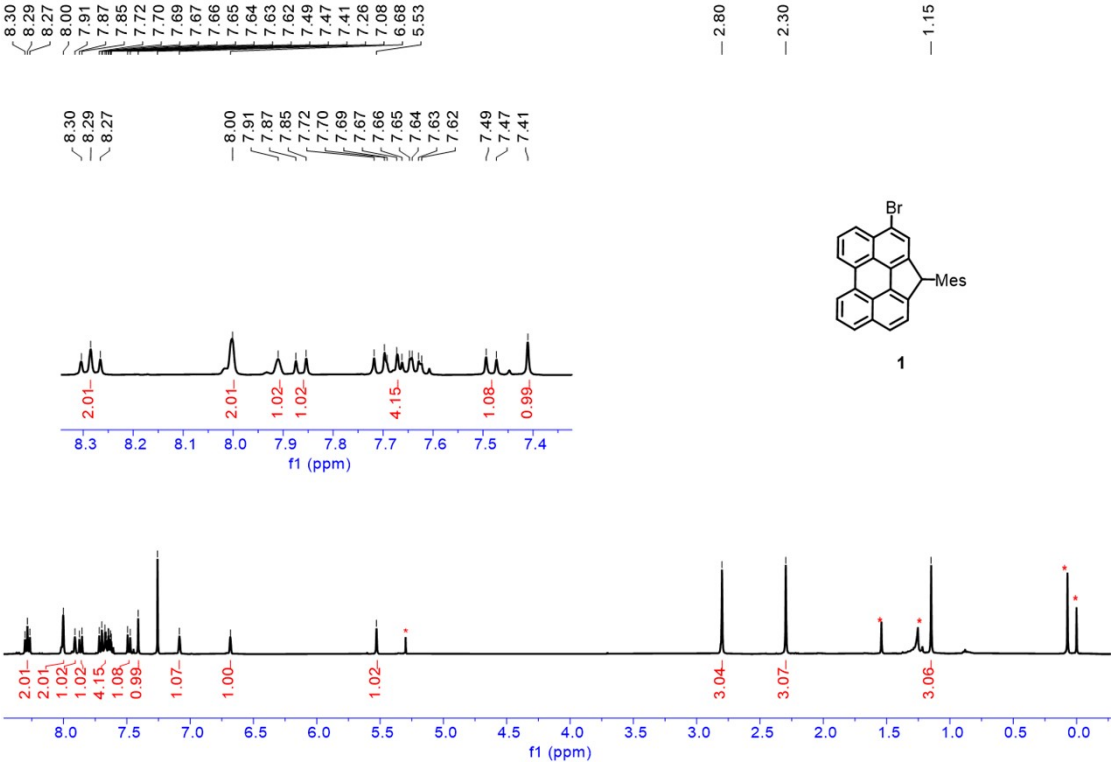

Figure S19. ^{1}H NMR (600 MHz) spectrum of compound **1** in $CDCl_3$. (* denotes the impurity from solvent).

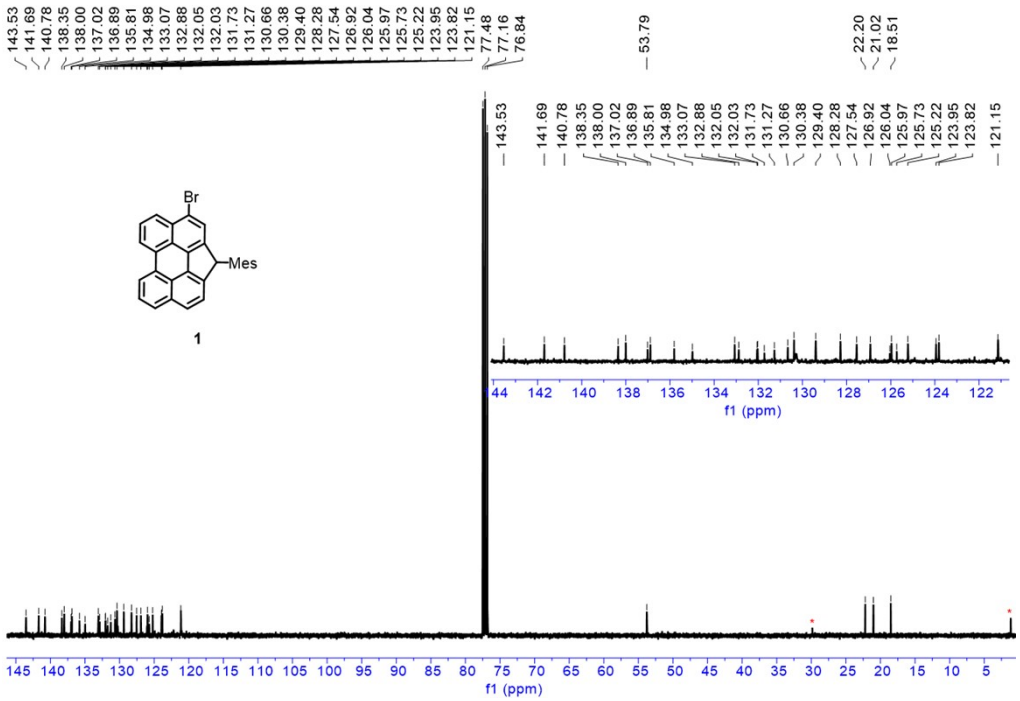

Figure S20. ^{13}C NMR (151 MHz) spectrum of compound **1** in $CDCl_3$. (* denotes the impurity from solvent).

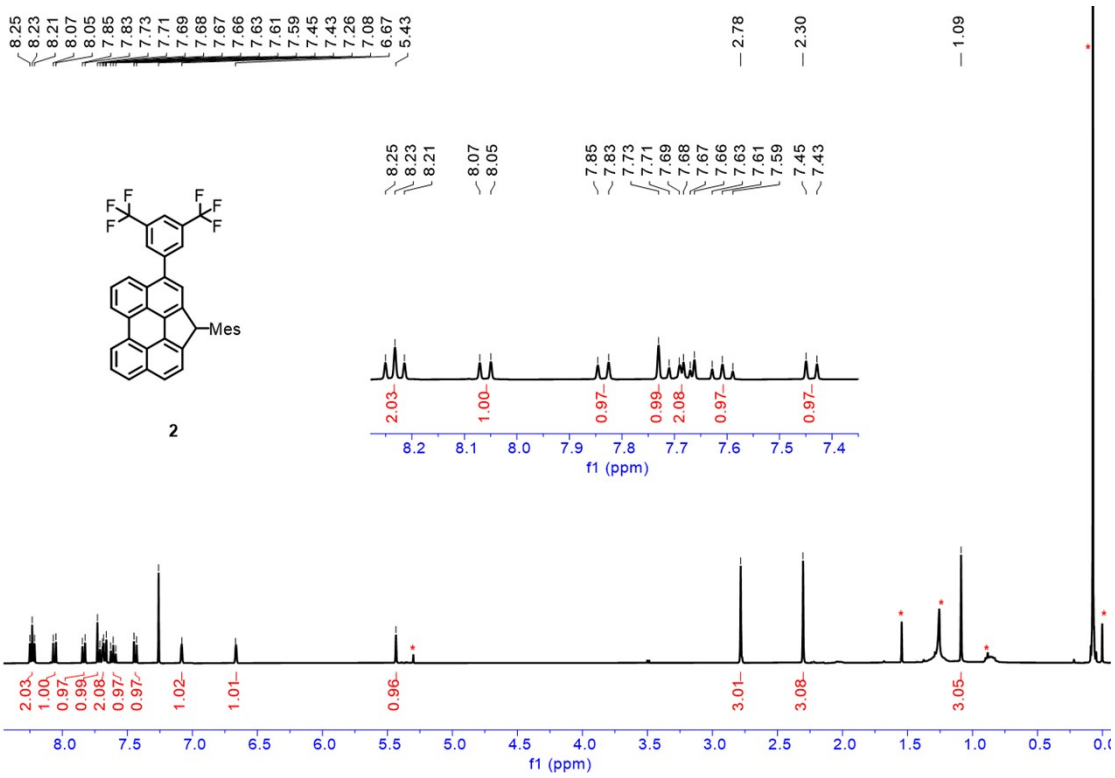

Figure S21. ^{1}H NMR (600 MHz) spectrum of compound **2** in $CDCl_3$. (* denotes the impurity from solvent).

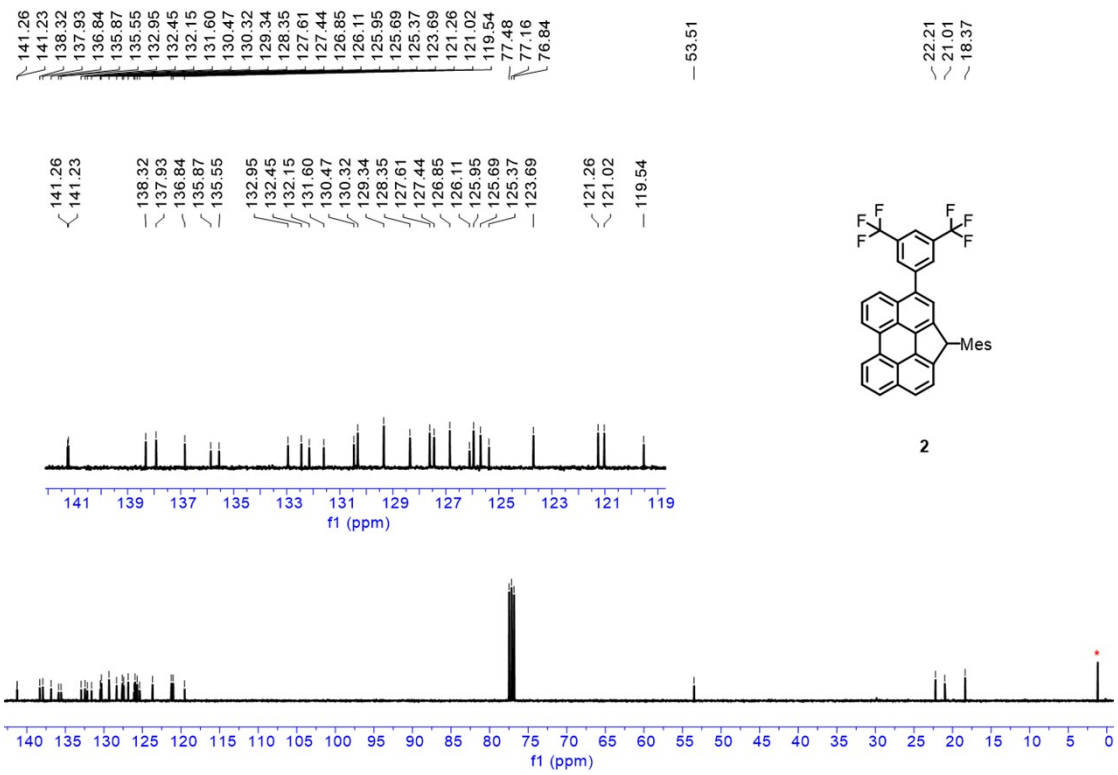

Figure S22. ^{13}C NMR (151 MHz) spectrum of compound **2** in $CDCl_3$. (* denotes the impurity from solvent).

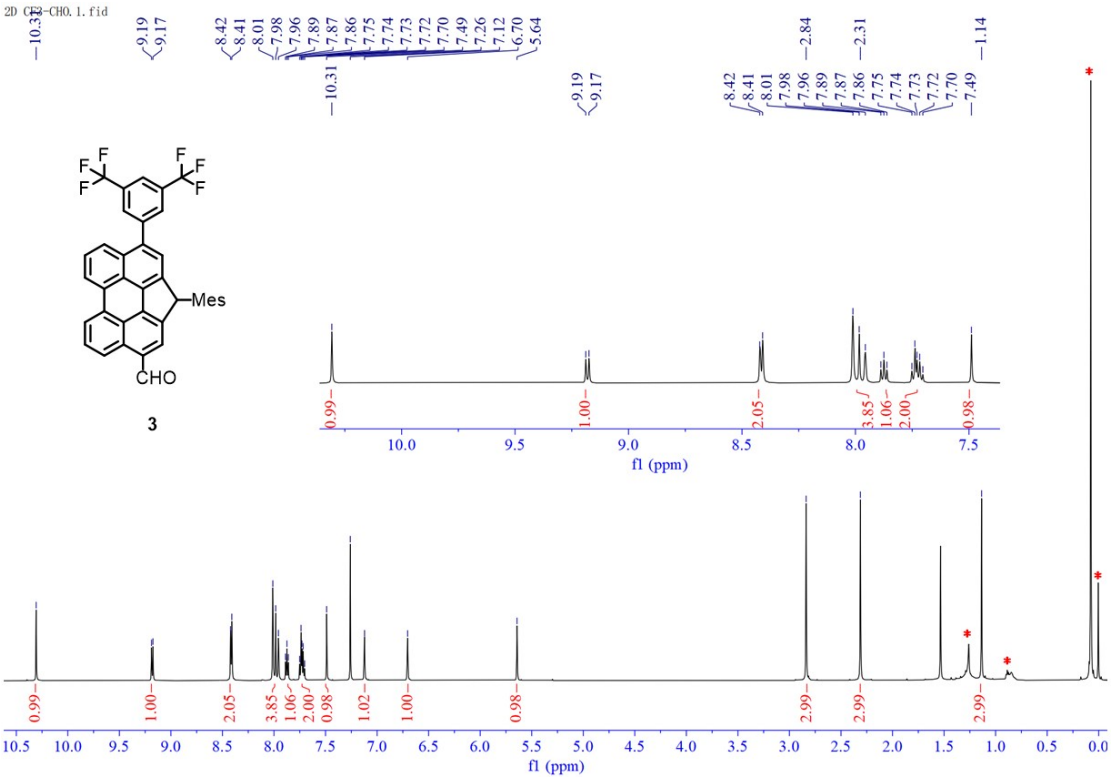

Figure S23. ^{1}H NMR (600 MHz) spectrum of compound **3** in $CDCl_3$. (* denotes the impurity from solvent).

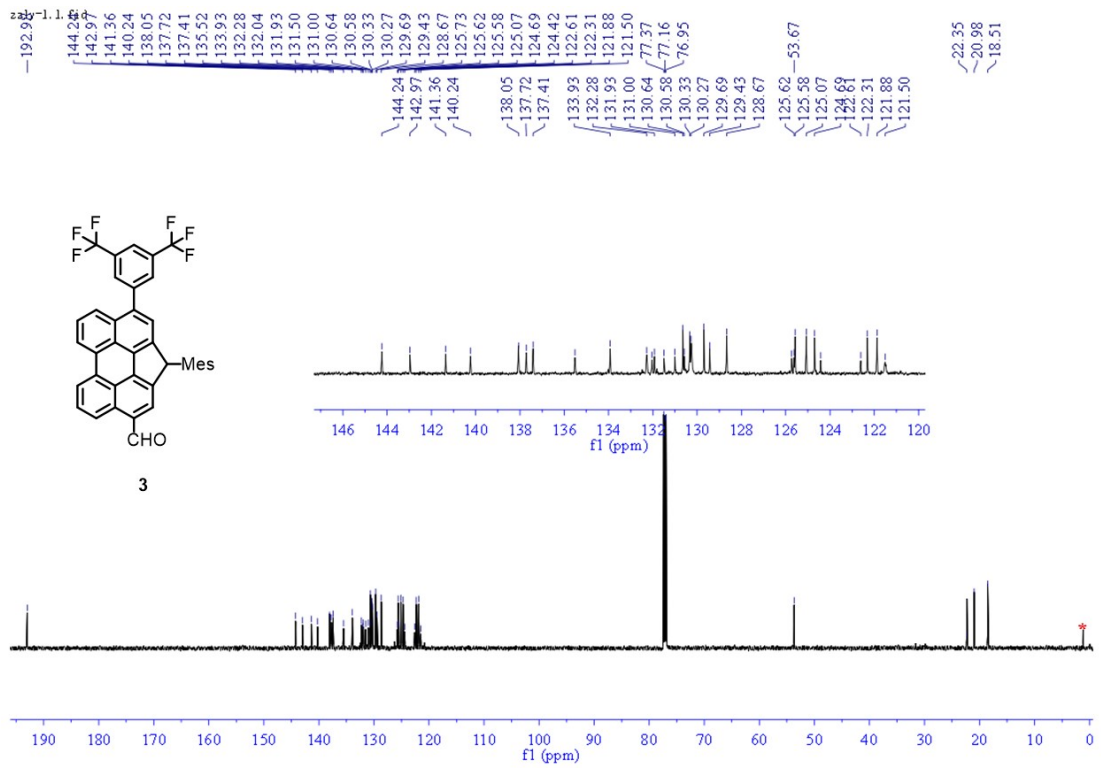

Figure S24. ^{13}C NMR (151 MHz) spectrum of compound **3** in $CDCl_3$. (* denotes the impurity from solvent).

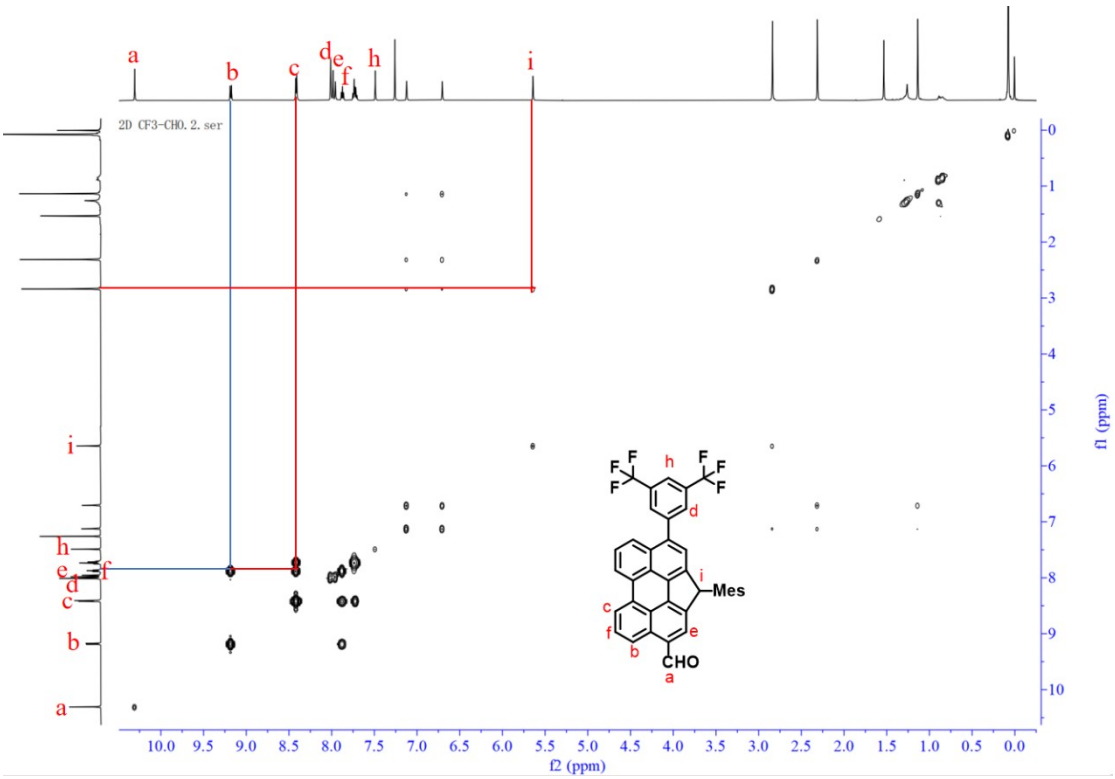

Figure S25. 2D COSY NMR (600 MHz) spectrum of compound **3** in $CDCl_3$.

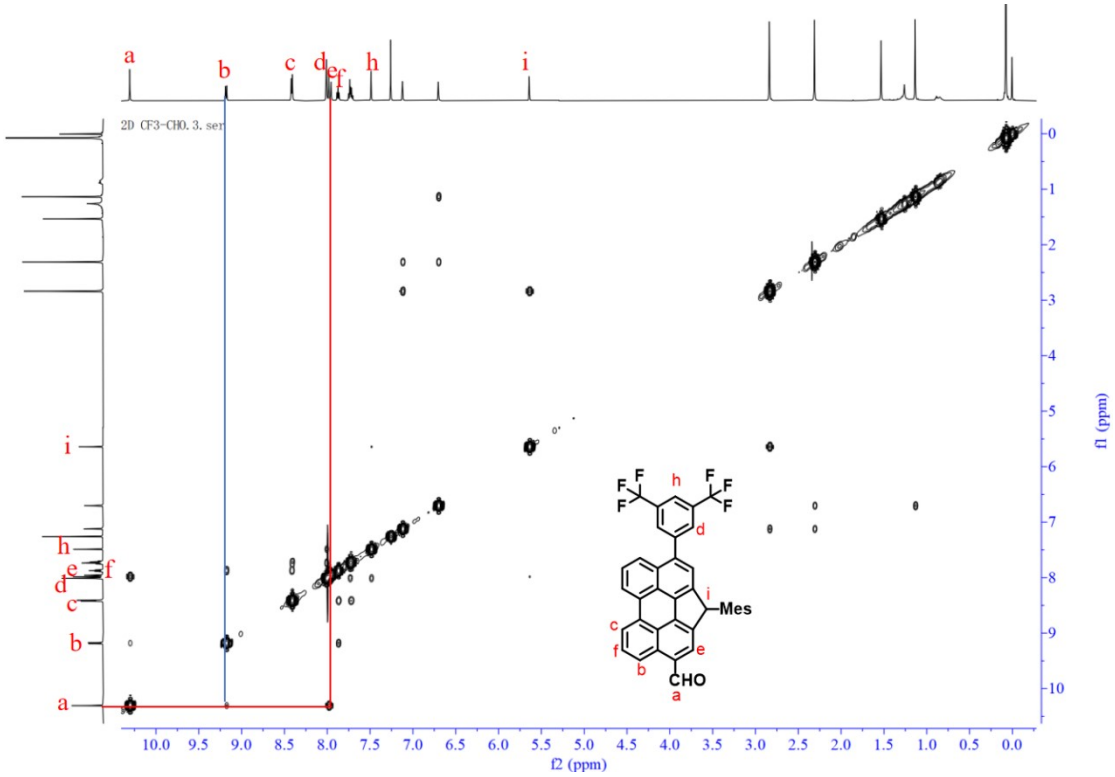

Figure S26. 2D NOESY NMR (600 MHz) spectrum of compound **3** in $CDCl_3$.

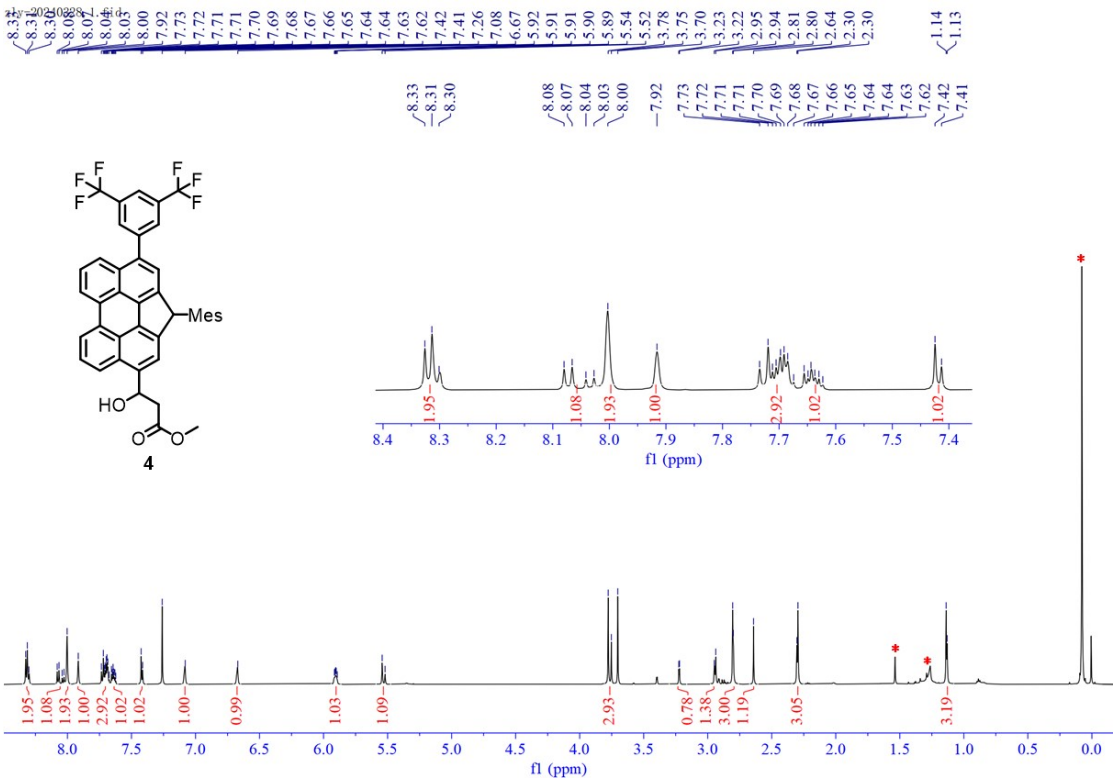

Figure S27. ^{1}H NMR (600 MHz) spectrum of compound **4** in $CDCl_3$. (* denotes the impurity from solvent).

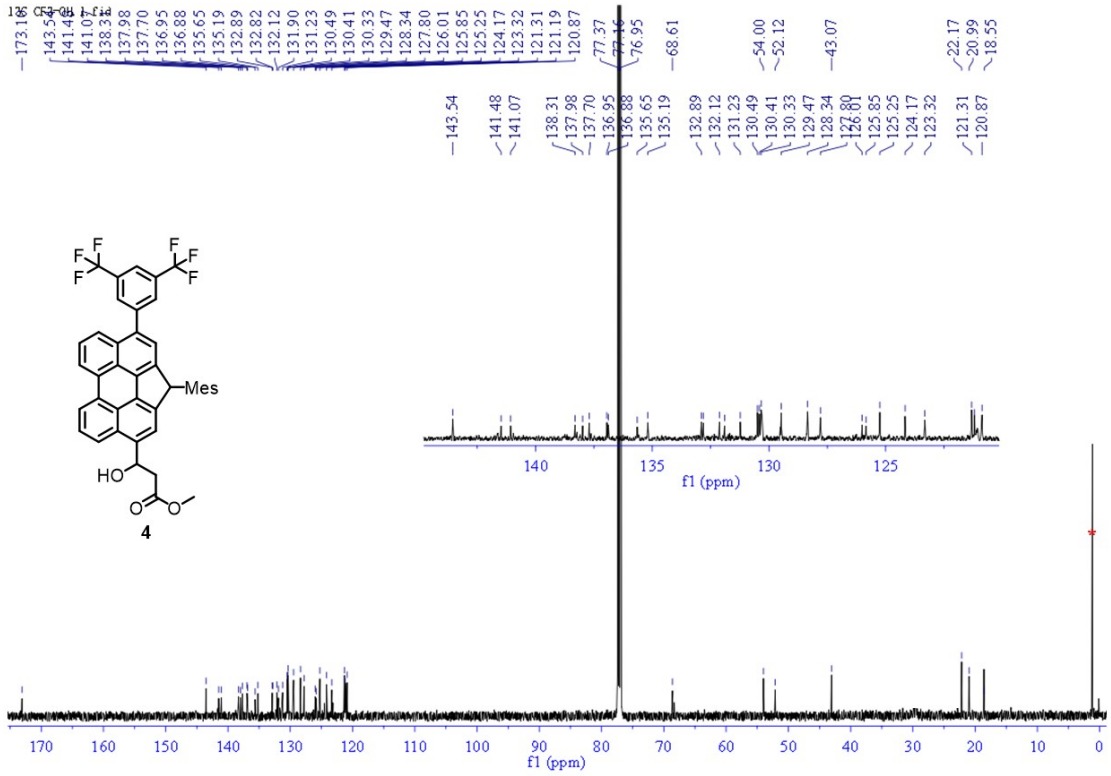

Figure S28. ^{13}C NMR (151 MHz) spectrum of compound **4** in $CDCl_3$. (* denotes the impurity from solvent).

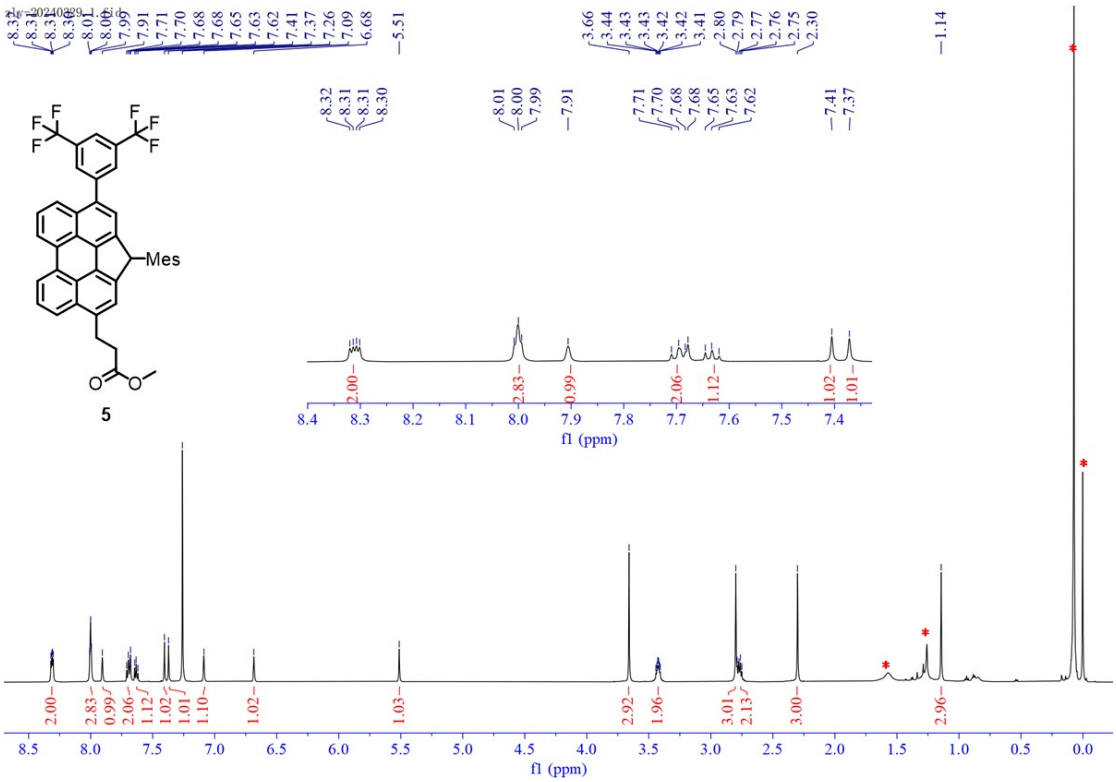

Figure S29. ^{1}H NMR (600 MHz) spectrum of compound **5** in $CDCl_3$. (* denotes the impurity from solvent).

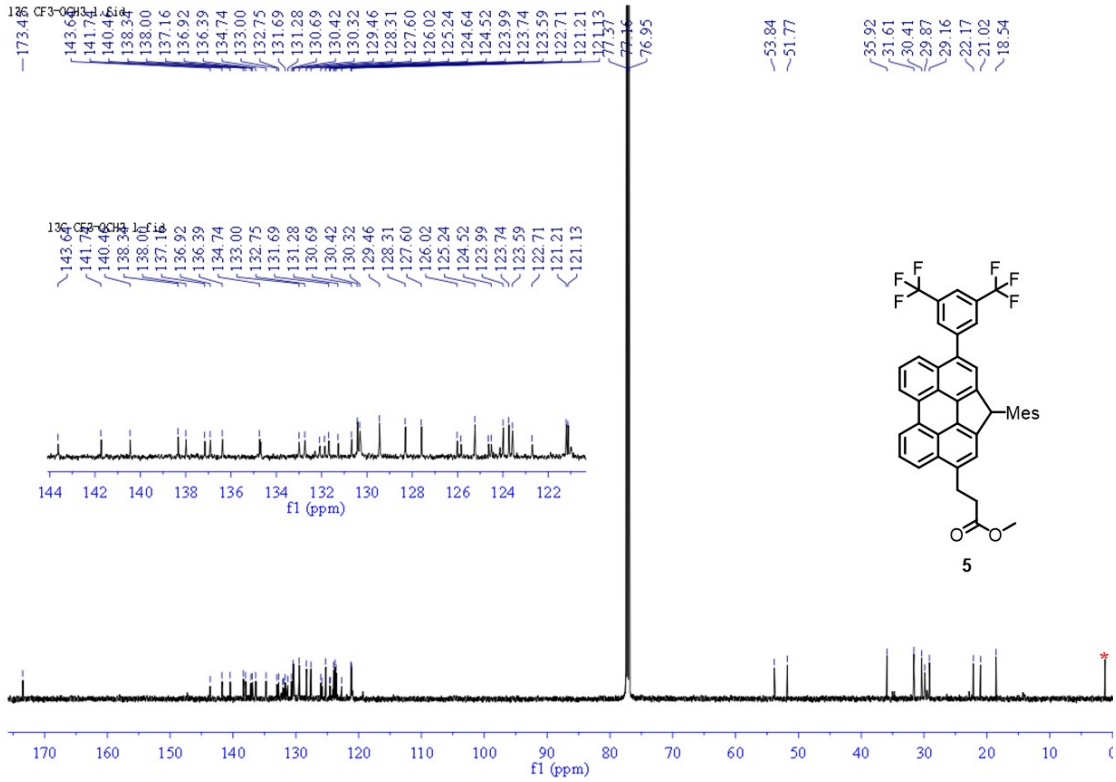

Figure S30. ^{13}C NMR (151 MHz) spectrum of compound **5** in $CDCl_3$. (* denotes the impurity from solvent).

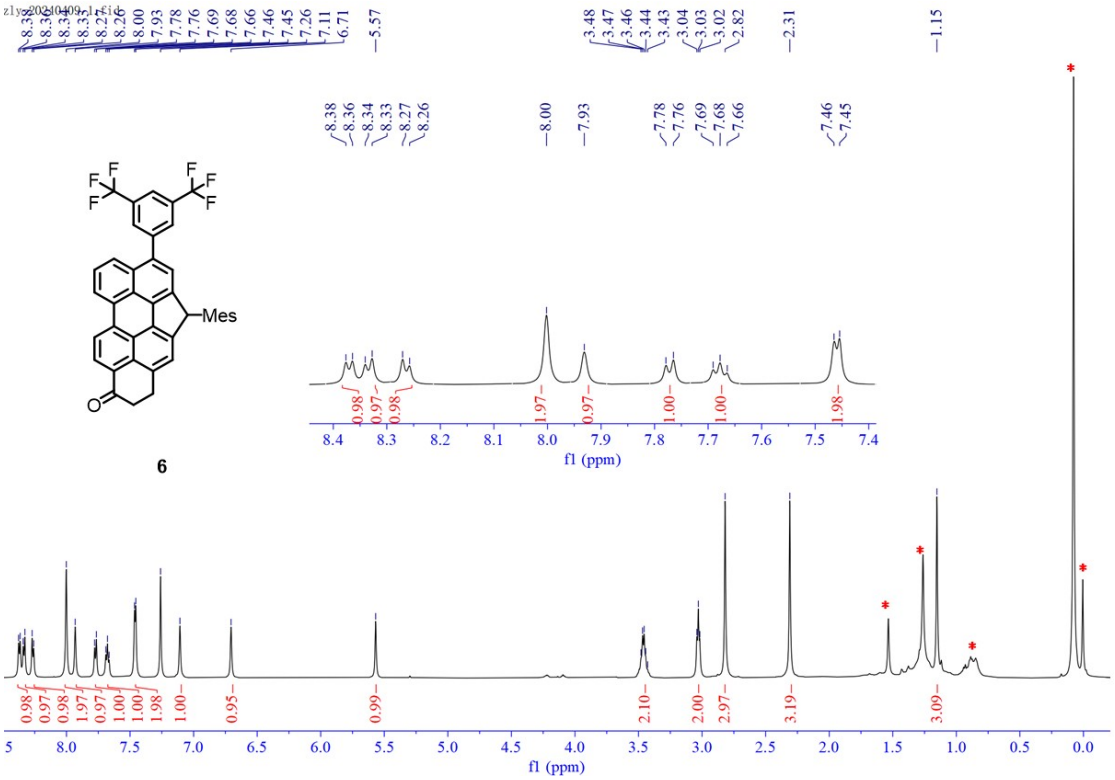

Figure S31. ^{1}H NMR (600 MHz) spectrum of compound **6** in $CDCl_3$. (* denotes the impurity from solvent).

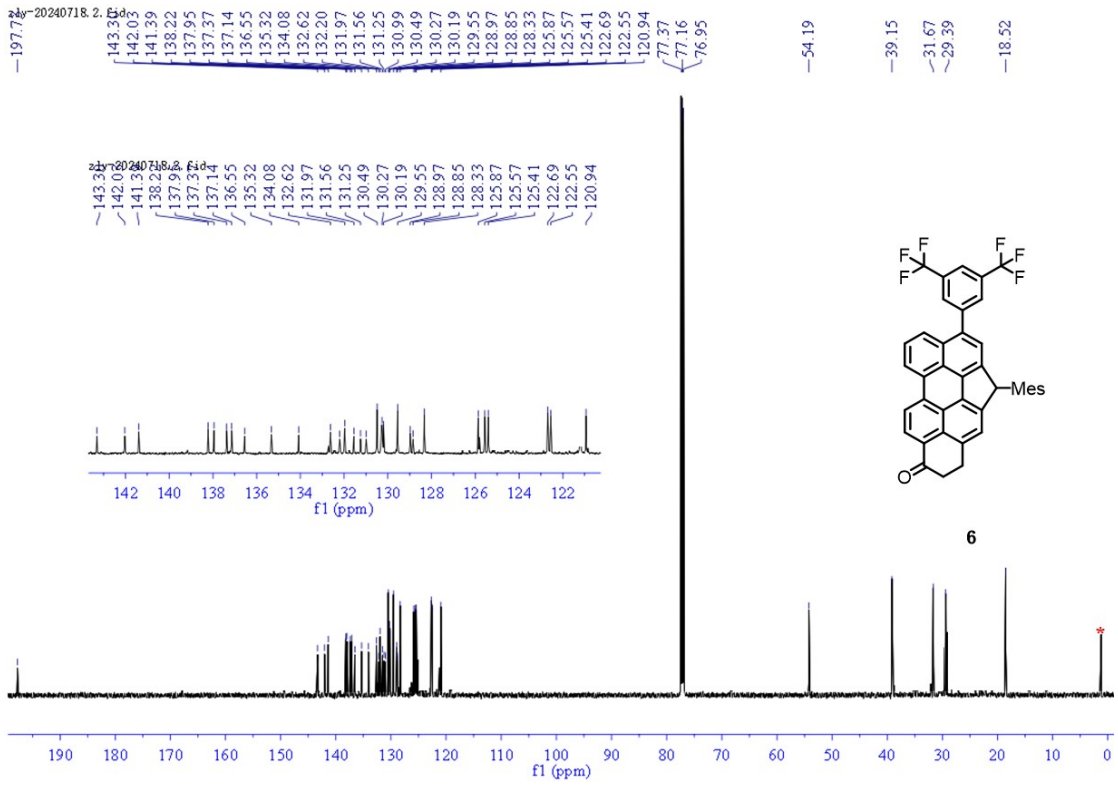

Figure S32. ^{13}C NMR (151 MHz) spectrum of compound **6** in $CDCl_3$. (* denotes the impurity from solvent).

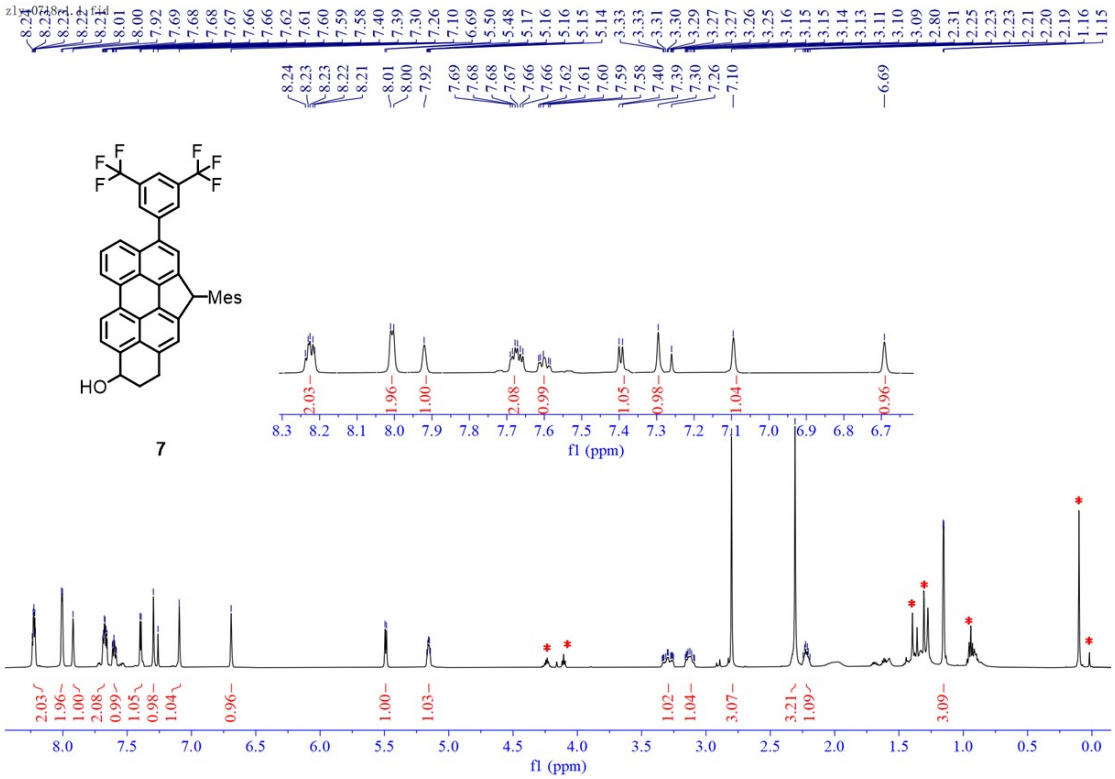

Figure S33. ^{1}H NMR (600 MHz) spectrum of compound **7** in $CDCl_3$. (* denotes the impurity from solvent).

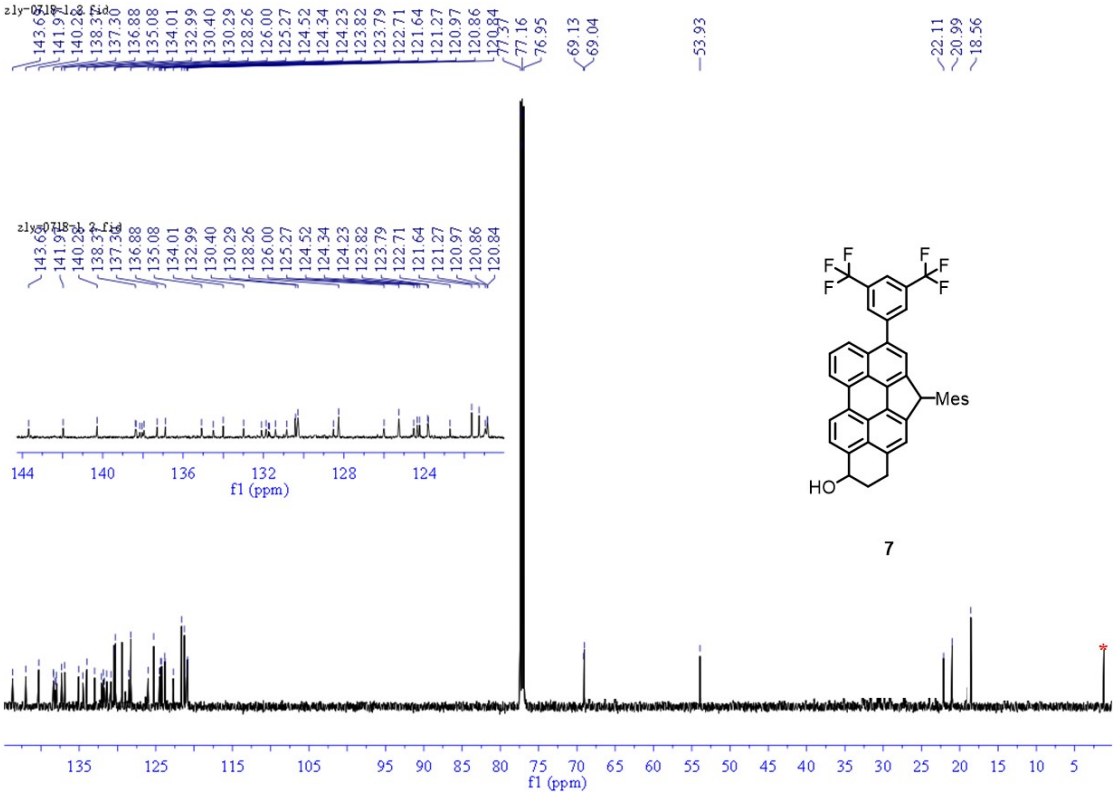

Figure S34. ^{13}C NMR (151 MHz) spectrum of compound **7** in $CDCl_3$. (* denotes the impurity from solvent).

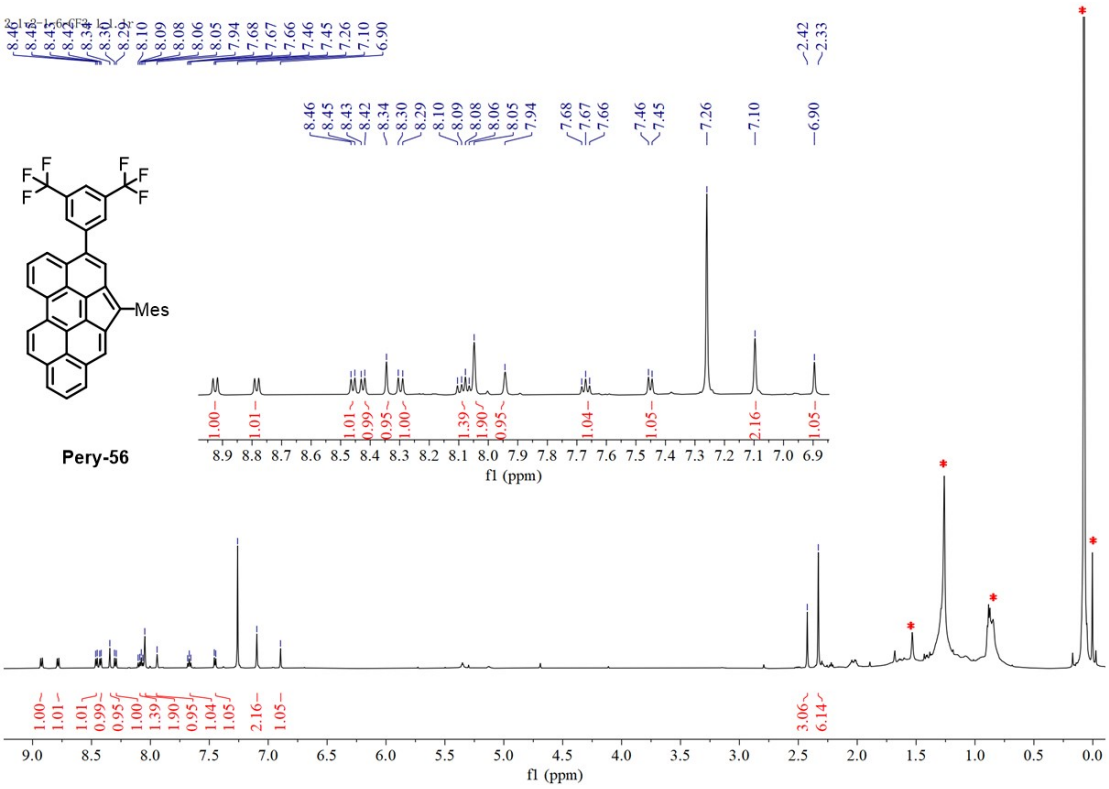

Figure S35. ^{1}H NMR (600 MHz) spectrum of compound **Pery-56** in $CDCl_3$. (* denotes the impurity from solvent).

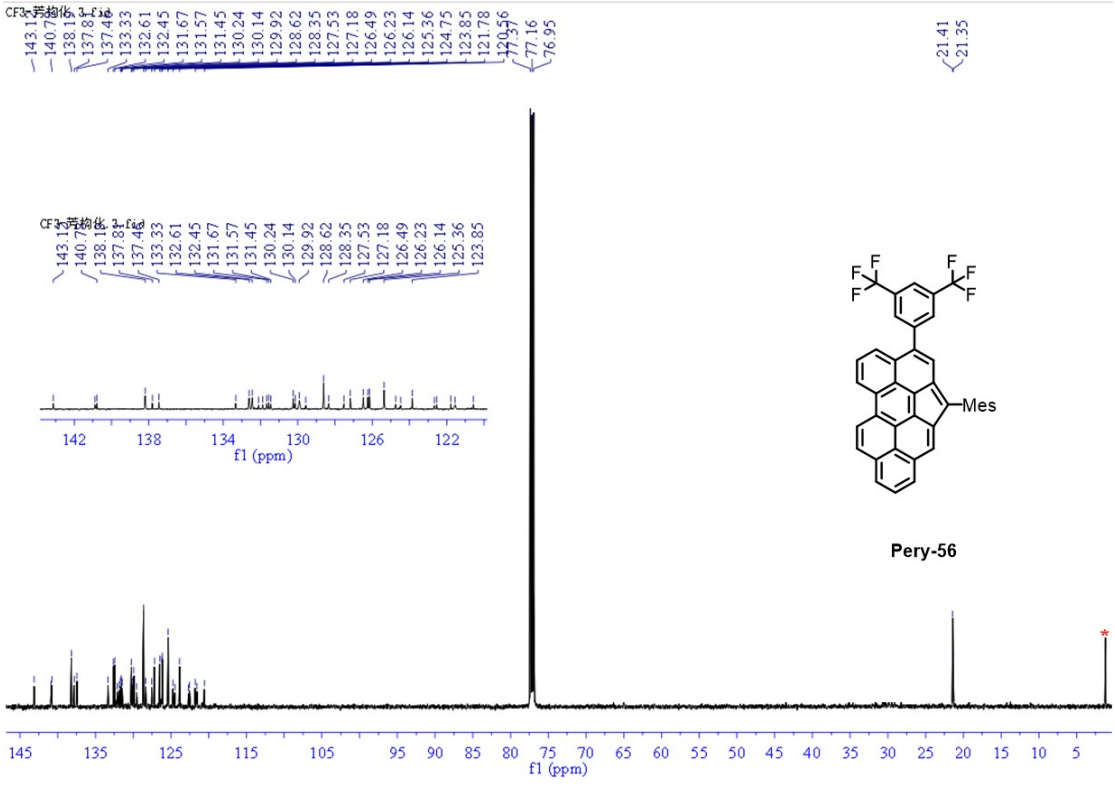

Figure S36. ^{13}C NMR (151 MHz) spectrum of compound **Pery-56** in $CDCl_3$. (* denotes the impurity from solvent).

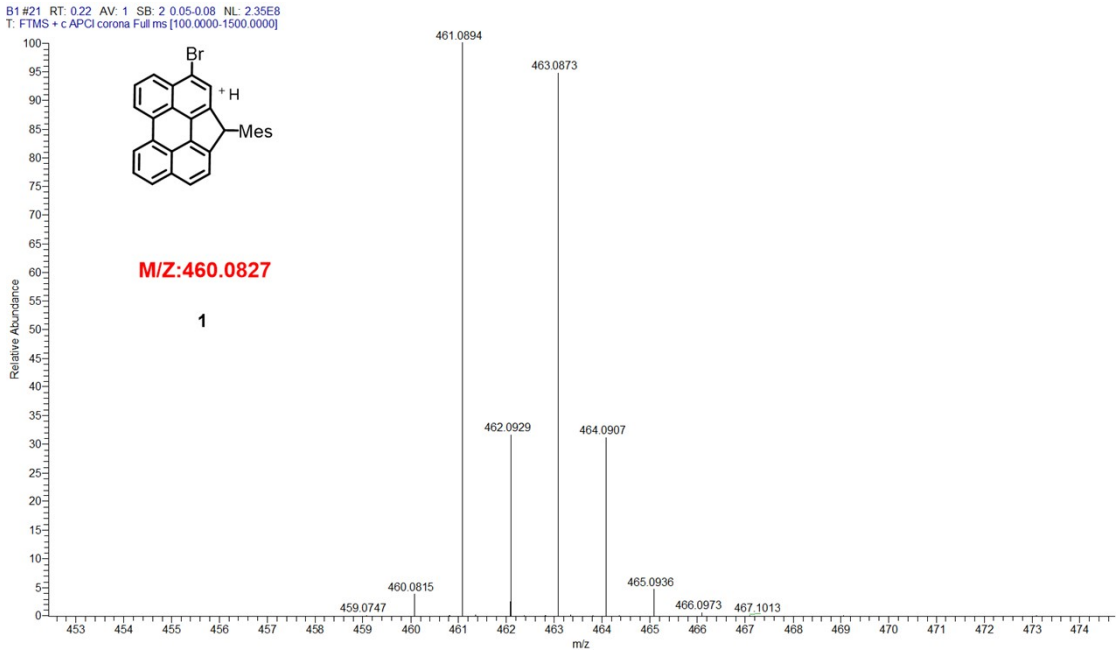

Figure S37. HR mass spectrum (APCI) of **1**.

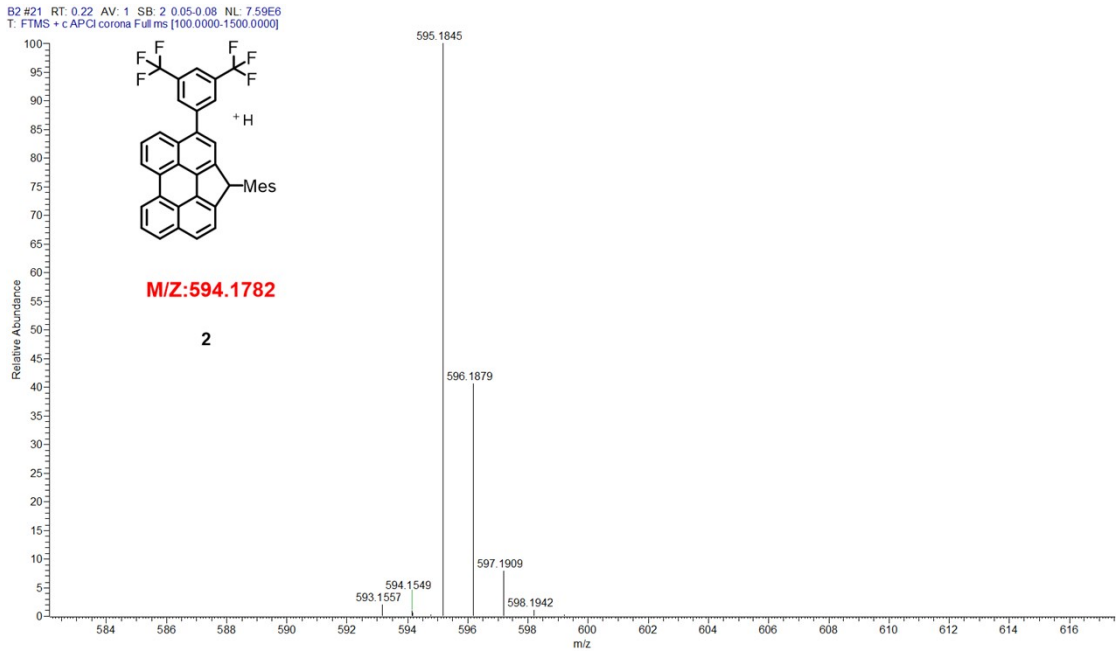

Figure S38. HR mass spectrum (APCI) of **2**.

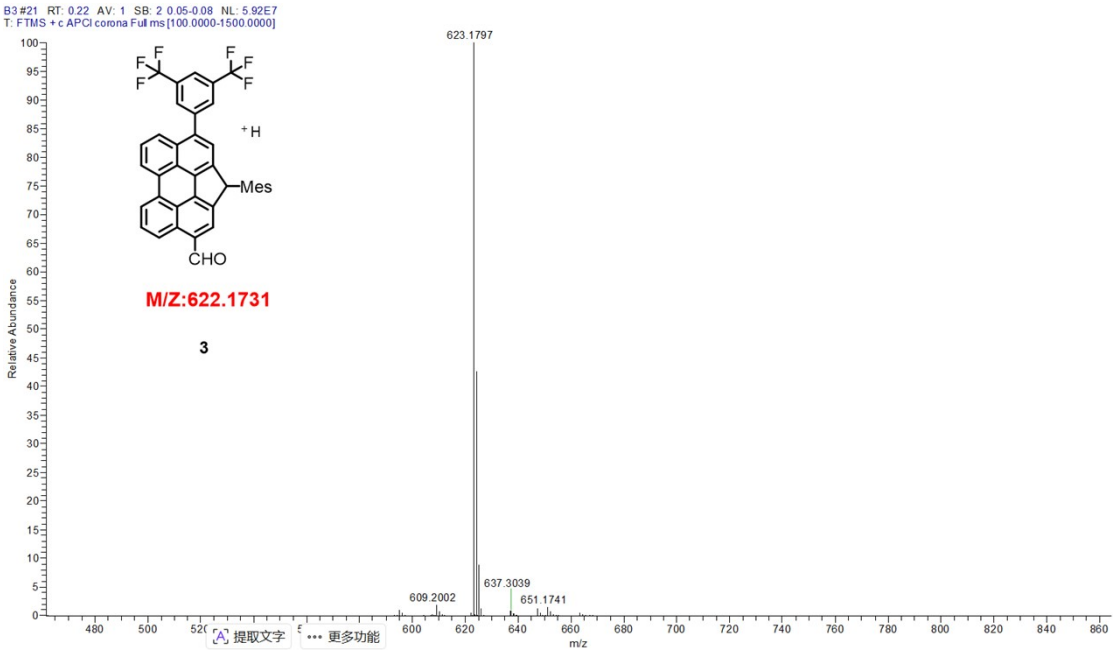

Figure S39. HR mass spectrum (APCI) of **3**.

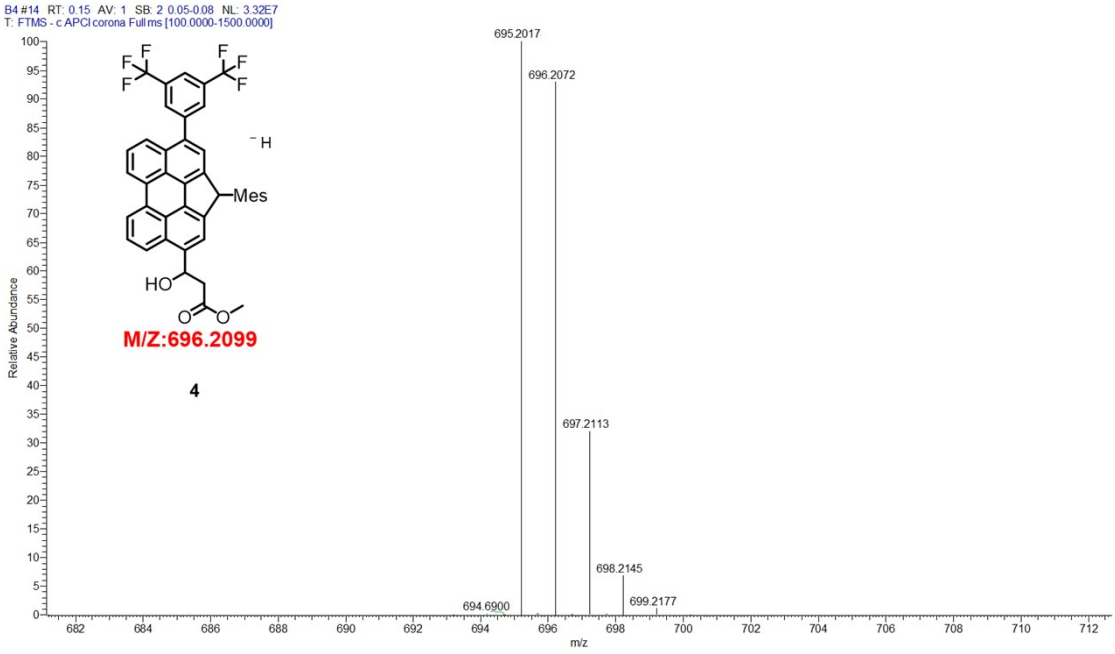

Figure S40. HR mass spectrum (APCI) of **4**.

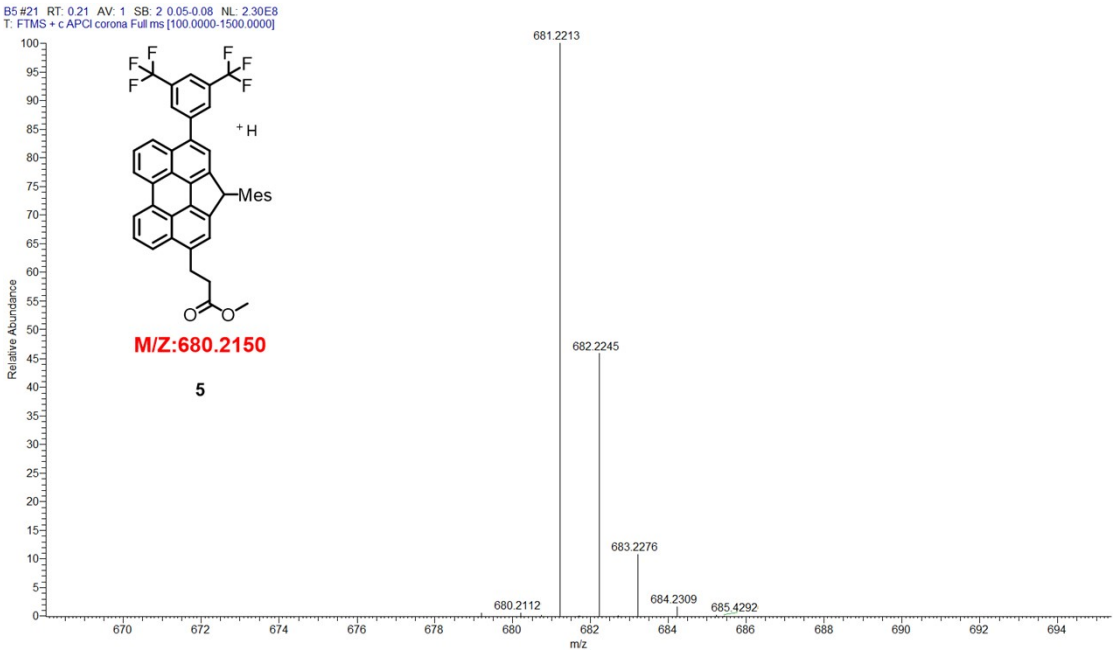

Figure S41. HR mass spectrum (APCI) of **5**

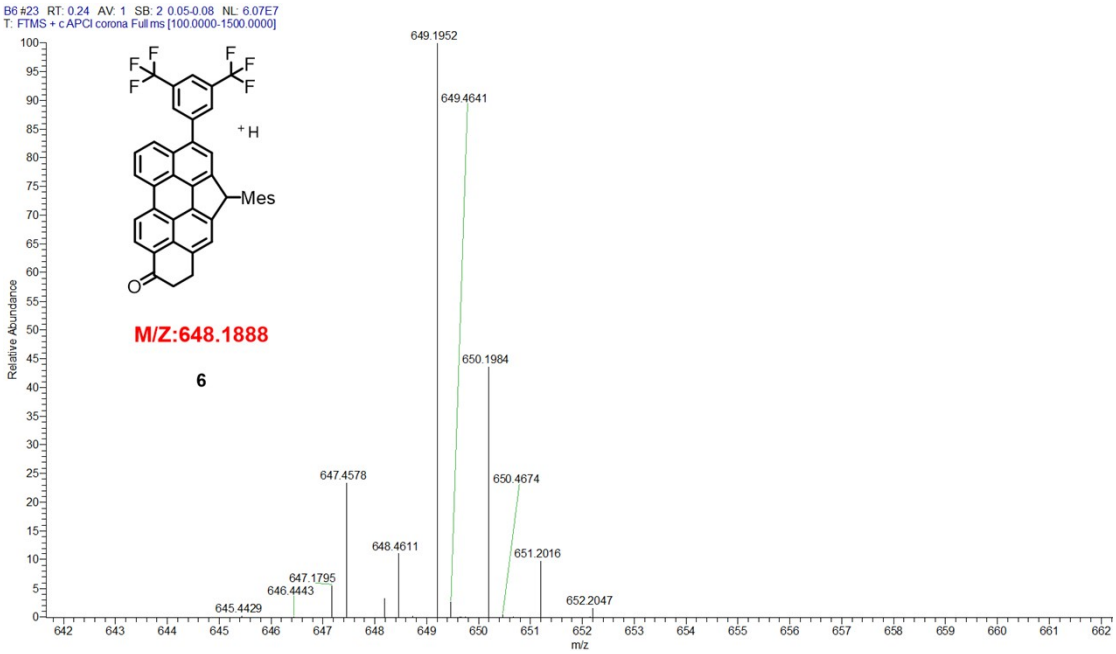

Figure S42. HR mass spectrum (APCI) of **6**

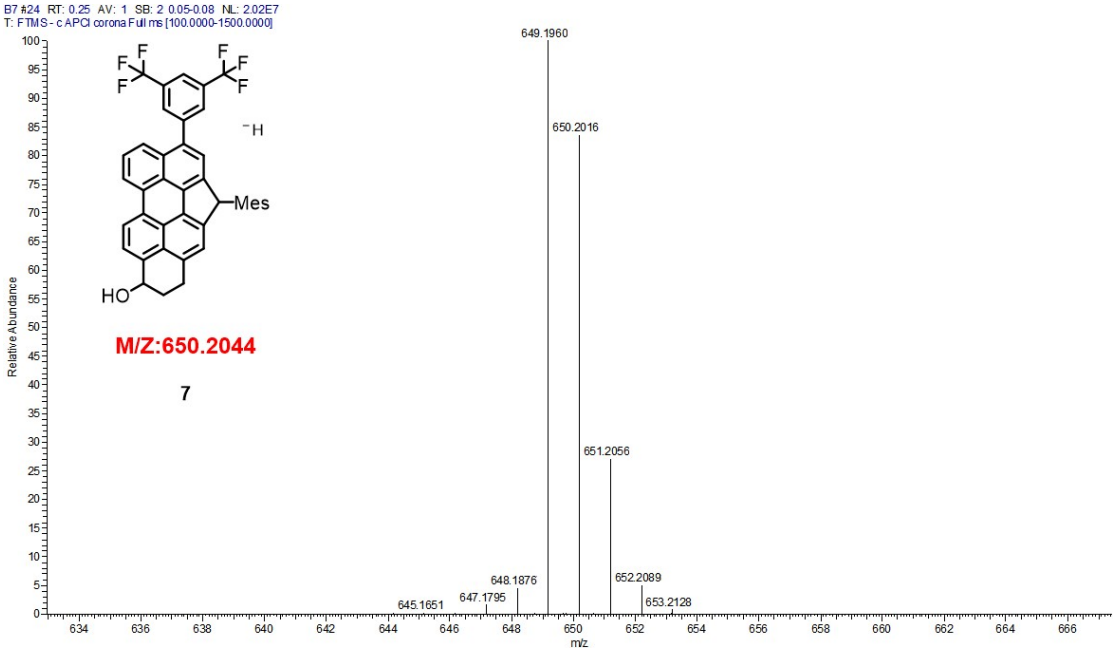

Figure S43. HR mass spectrum (APCI) of **7**

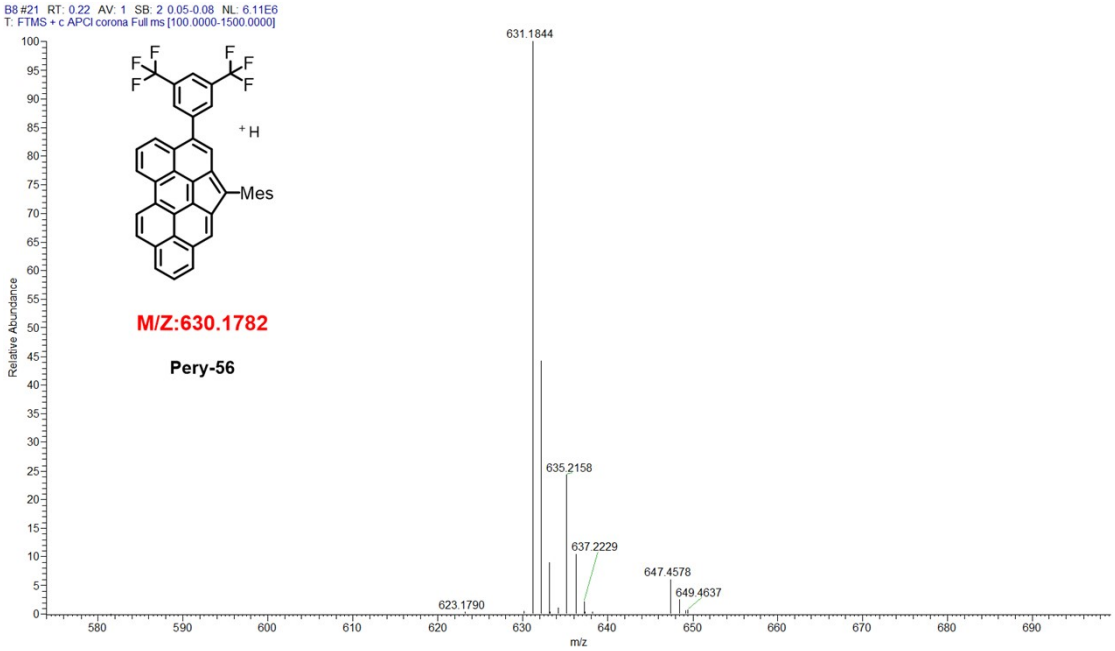

Figure S44. HR mass spectrum (APCI) of **Pery-56**

6. Reference

[1] M. J. Frisch, G. W. Trucks, H. B. Schlegel, G. E. Scuseria, M. A. Robb, J. R. Cheeseman, G. Scalmani, V. Barone, G. A. Petersson, H. Nakatsuji, X. Li, M. Caricato, A. V. Marenich, J. Bloino, B. G. Janesko, R. Gomperts, B. Mennucci, H. P. Hratchian, J. V. Ortiz, A. F. Izmaylov, J. L. Sonnenberg, Williams, F. Ding, F. Lipparini, F. Egidi, J. Goings, B. Peng, A. Petrone, T. Henderson, D. Ranasinghe, V. G. Zakrzewski, J. Gao, N. Rega, G. Zheng, W. Liang, M. Hada, M. Ehara, K. Toyota, R. Fukuda, J. Hasegawa, M. Ishida, T. Nakajima, Y. Honda, O. Kitao, H. Nakai, T. Vreven, K. Throssell, J. A. Montgomery Jr., J. E. Peralta, F. Ogliaro, M. J. Bearpark, J. J. Heyd, E. N. Brothers, K. N. Kudin, V. N. Staroverov, T. A. Keith, R. Kobayashi, J. Normand, K. Raghavachari, A. P. Rendell, J. C. Burant, S. S. Iyengar, J. Tomasi, M. Cossi, J. M. Millam, M. Klene, C. Adamo, R. Cammi, J. W. Ochterski, R. L. Martin, K. Morokuma, O. Farkas, J. B. Foresman, D. J. Fox, *Gaussian 16 Rev. C.01*, Wallingford, CT, **2016**.

[2] T. Lu, F. Chen, *J. Comput. Chem.* **2012**, *33*, 580.

[3] T. Lu, F. Chen, *J. Mol. Graph. Model.* **2012**, *38*, 314.

[4] a) A. D. Becke, *J. Chem. Phys.* **1993**, *98*, 5648; b) C. Lee, W. Yang, R. G. Parr, *Phys. Rev. B: Condens. Matter.* **1988**, *37*, 785; c) T. Yanai, D. Tew, N. Handy, *Chem. Phys. Lett.* **2004**, *393*, 51; d) R. Ditchfield, W. J. Hehre, J. A. Pople, *J. Chem. Phys.* **1971**, *54*, 724; e) W. J. Hehre, R. Ditchfield, J. A. Pople, *J. Chem. Phys.* **1972**, *56*, 2257; f) P. C. Hariharan, J. A. Pople, *Theor. Chim. Acta*. **1973**, *28*, 213.

[5] a) S. Yamanaka, M. Okumura, M. Nakano, K. Yamaguchi, *J. Mol. Struct.* **1994**, *310*, 205; b) K. Kamada, K. Ohta, A. Shimizu, T. Kubo, R. Kishi, H. Takahashi, E. Botek, B. Champagne, M. Nakano, *J. Phys. Chem. Lett.* **2010**, *1*, 937.

[6] Z. Chen, C. S. Wannere, C. Corminboeuf, R. Puchta, P. v. R. Schleyer, *Chem. Rev.* **2005**, *105*, 3842.

[7] D. Geuenich, K. Hess, F. Köhler, R. Herges, *Chem. Rev.* **2005**, *105*, 3758.

[8] W. Humphrey, A. Dalke, K. Schulten, *J. Mol. Graph.* **1996**, *14*, 33.